Compartmentalized input-output organization of Lugaro cells in the cerebellar cortex

Taisuke Miyazaki[1,2], Miwako Yamasaki[1], Kenji F. Tanaka[3], Masahiko Watanabe[1]

[1]Department of Anatomy, Faculty of Medicine, [2]Department of Functioning and Disability, Faculty of Health Sciences, Hokkaido University, Sapporo 060-8638, Japan, and [3]Department of Neuropsychiatry, Keio University School of Medicine, Tokyo 160-8582, Japan

Short title: Cerebellar Lugaro cell

Correspondence and proofs to: Taisuke Miyazaki and Masahiko Watanabe
Department of Functioning and Disability, Faculty of Health Sciences (TM), Department of Anatomy, Faculty of Medicine (MW), Hokkaido University Sapporo 060-8638, Japan.
TEL: +81-11-706-3330 (TM), +81-11-706-5030 (MW); FAX: +81-11-706-5031 (MW);
e-mail: miyazaki@med.hokudai.ac.jp (TM), watamasa@med.hokudai.ac.jp (MW)

Key Words: Lugaro cell, globular cell, Purkinje cell, transgenic mouse, cerebellar compartment

50 Text Pages with 7 Figures and 2 Tables.

Number of words: Abstract, 250; Significance Statement, 120; Introduction, 639;

Discussion 1489

Acknowledgements

We thank Naoki Hidaka and Kazuo Kitamura in University of Yamanashi for the participation in the preliminary experiments. This study was supported by Grant-in-Aid for Scientific Research (C) from the Ministry of Education, Culture, Sports, Science and Technology of Japan (MEXT) to T. M (17K08485) and Y. M (17K08503), the Narishige Neuroscience Research Foundation to T. M., and Takeda Science foundation to T. M.

The authors declare no competing financial interests.

Abstract

Purkinje cells (PCs) are principal cerebellar neurons, and several classes of interneurons modulate their activity. Lugaro cells (LCs) are one such inhibitory interneuron with distinctive cytology and location, but still most enigmatic among cerebellar neurons. Here we serendipitously produced a novel transgenic mouse line, where a half of Yellow Cameleon (YC)(+) cells in the cerebellar cortex were judged to be LCs, and YC(+) LCs were estimated to constitute one-third of the total LC populations. Neurochemically, two-thirds of YC(+) LCs were dually GABAergic/glycinergic, with the rest being GABAergic. Beneath the PC layer, they extended a sheet of somatodendritic meshwork interconnected with neighboring LCs by adherens junctions, and received various inputs from climbing fibers, mossy fibers, granule cell axons, recurrent PC axons, Golgi cell axons, LC axons, and serotonergic fibers. Intriguingly, somatodendritic elements of individual LCs preferentially extended within a given cerebellar compartment defined by aldolase C expression. In turn, YC(+) LCs projected a dense lattice of ascending and transverse axons to the molecular layer, and innervated molecular layer interneurons (basket and stellate cells) and Golgi cells, but not PCs. Of note, ascending axons profusely innervated individual targets within a cerebellar compartment, while transverse axons ran across several compartments and innervated targets sparsely. This unique circuit configuration highlights that LCs integrate various excitatory, inhibitory, and modulatory inputs coming to the belonging cerebellar compartment and that, as an interneuron-selective interneuron, LCs can effectively disinhibit cerebellar cortical activities in a compartment-dependent manner through inhibition of inhibitory interneurons selectively targeting PCs and

granule cells.

Introduction

Purkinje cells (PCs) integrate enormous inputs and, as the sole output neurons in the cerebellar cortex, project to the cerebellar and vestibular nuclei. PC dendrites are arborized in the parasagittal plane of the molecular layer, and receive two orthogonal excitatory afferents (Palay and Chan-Palay, 1974). Climbing fibers (CFs) originating from the inferior olive establish mono-innervation to PCs by climbing up proximal dendrites and forming hundreds of synapses there (Kano and Watanabe, 2013). Cerebellar granule cells receive mossy fiber (MF) inputs from the brainstem and spinal cord, and emit a T-shaped axon consisting of the ascending axon and parallel fiber (PF). As running transversely in the molecular layer, 10^5 or more PFs innervate distal dendrites of individual PCs (Napper and Harvey, 1988; Kurihara et al., 1997). Conjunctive activation of CF and PF inputs induces long-term depression at PF-PC synapses, which is thought to underlie cerebellar motor learning (Ito et al., 2014).

PC output is modulated either directly or indirectly by several classes of inhibitory interneurons. Basket and stellate cells are molecular layer interneurons, which receive excitatory inputs from PFs synaptically and CFs via glutamate spillover, and project GABAergic outputs to PCs (Szapiro and Barbour, 2007). Basket cell axons embrace the soma and axon initial segment to regulate PC firing through GABAergic and electrical inhibitions (Korn and Axelrad, 1980; Gabbott et al., 1986; Iwakura et al., 2012; Blot and Barbour, 2014). Stellate cells innervate PC dendrites to counterbalance PF excitation and modulate local synaptic integration important in learning (Bower, 2010). They share similar developmental, molecular, and firing profiles, and represent a gradually varying cellular continuum (Watanabe, 2016).

There are, at least, three types of inhibitory granular layer interneurons, the Golgi cell, Lugaro cell (LC), and globular cell. Of these, Golgi cells are well studied at the cellular, circuit, and functional levels (Golgi, 1879; Eccles et al., 1967; Palay and Chan-Palay, 1974; Watanabe et al., 1998; Simat et al., 2007; Eyre and Nusser, 2016). Despite molecular diversity (Simat et al., 2007), Golgi cells share the commonality in that they are distributed throughout the granular layer, and have large polygonal soma, dendrites extending into the molecular layer, and axons arborizing in the granular layer. Golgi cells receive excitatory MFs and PFs, and provide the sole inhibitory (GABAergic/glycinergic) output to granule cells via the feed-forward and feed-back loops.

LCs and globular cells can be identified from distinctive cytological features. LCs have fusiform soma lying just beneath the PC layer, extend X-shaped horizontal dendrites beneath PC somata, and project ascending and transverse axons to the molecular layer (Lugaro, 1894; Rogers, 1989; Sahin and Hockfield, 1990; Arai et al., 1991; Floris et al., 1994; Laine and Axelrad, 2002). LCs are densely innervated by recurrent PC axons, and form GABAergic/glycinergic synapses on to basket, stellate, and Golgi cells, but never on PCs (Lemkey-Johnston and Larramendi, 1968; Palay and Chan-Palay, 1974; Laine and Axelrad, 2002; Simat et al., 2007). Globular cells place their small globular soma in the granular layer and extend dendrites and axons to the molecular layer. From their similar location, calretinin (CR) expression, and axonal projection, LCs and globular cells are thought to be a cellular continuum (Laine and Axelrad, 2002). Nevertheless, these interneurons are often neglected from the cerebellar circuit map, like missing pieces in the jigsaw puzzle. This is partly due to insufficient understanding of their input-output relationships in cerebellar circuits. For example, the source of excitatory inputs that drives

these interneurons to fire remains largely unknown. Moreover, while circuit connections of the other interneurons are subjected to longitudinal cerebellar compartmentalization (Consalez and Hawkes, 2013), nothing is known for LCs

Using a novel reporter mouse line in which Yellow Cameleon (YC) is preferentially expressed in LCs and globular cells, we anatomically examined neurochemical and input-output properties of YC(+) LCs, and also pursued the extent of dendritic and axonal arborizations in relation with cerebellar compartments.

Experimental Procedures

Generation of D118-YC mice

A cassette containing mammalianized tetracycline transcriptional activator (tTA)-SV40 polyadenylation signal was inserted into the translation initiation site of the dopamine receptor type 1 (*Drd1*) gene in mouse bacterial artificial chromosome (BAC) DNA (clone RP23-322H10) (Fig 1A, B). Modified linearized BAC DNA was injected into fertilized eggs from CBA/C57BL6 mice. Ten founder lines were obtained and all lines were crossed with tetO-YC knockin mice (Kanemaru et al., 2014) to confirmed tTA-mediated gene induction (Fig. 1C). In all double transgenic lines (*Drd1*-tTA::tetO-YC), YC induction in the striatum was observed as expected. While transgene induction can be turned off by administration of doxycycline, we used the system solely to achieve promoter-specific and sufficient expression of YC. From 10 lines of the double transgenic mice, the *Drd1*-tTA line 18 was selected and named D118-YC mice.

The following primer set: D1R-423U (5’- TAGGGCATTTGGAGAGATGTGGCA-3’)

and mtTA24L (5'-CGGAGTTGATCACCTTGGACTTGT-3') was used in genotyping for *Drd1*-tTA mice. Transgenic mice yielded a 450 bp band and wild type mice did not. Genotyping for tetO-YC was described elsewhere (Kanemaru et al., 2014). *Drd1*-tTA::tetO-YC bigenic mice were fed with normal chow (CE-2, CLEA). All mice were maintained with 12:12-h light/dark cycle (lights on at 8 am). Mice at 2 months of age were used as adult mice, unless otherwise noted.

Animal fixation and section preparation

Under deep pentobarbital anesthesia (150 mg/kg of body weight, i.p.), mice for light microscopic immunohistochemistry and anterograde tracer labeling were perfused transcardially with 4% paraformaldehyde in 0.1 M sodium phosphate buffer (PB, pH 7.2), while those for immunoelectron microscopy were perfused with 4% paraformaldehyde-0.1% glutaraldehyde in PB. Cerebellar sections in the sagittal, coronal, and horizontal planes were prepared on a microslicer (VT1000S; Leica). The thickness of sections was 50 μm.

Antibodies

We used affinity-purified primary antibodies, and the information on antigen sequence, host species, specificity, RRID, and references are summarized in Table 1. GFP antibody was used to detect YC. We raised antibodies to mouse CR in the rabbit and to DsRed in the rabbit and guinea pig. The specificity of DsRed antibodies was shown by specific immunohistochemical labeling in DsRed-introduced mice but not in wild-type mice. The specificity of CR antibody was shown by specific immunohistochemical labeling in interneurons of the hippocampus, cortex, and striatum and immunoblot labeling of 30 kDa band in brain homogenates.

Immunofluorescence

All incubations in immunofluorescence were done at room temperature in a free-floating state. Phosphate-buffered saline (PBS) was used as diluent buffer of blocking serum and antibodies and washing buffer. Cerebellar sections were incubated successively with 10% normal donkey serum for 20 min, a mixture of primary antibodies overnight at 1 μg/ml each, and a mixture of Alexa Fluor 405-, Alexa Fluor 488- (Invitrogen), indocarbocyanine (Cy3)- and indodicarbocyanine (Cy5)-labeled species-specific secondary antibodies (Jackson ImmunoResearch) for 2 h at a dilution of 1:200. Confocal images were taken with a laser scanning microscope (FV1000, FV1200; Olympus) equipped with a helium–neon/argon laser and with PlanApo (10x/0.40), UPLFLN (40x/1.30, oil immersion), and PlanApoN (60x/1.42, oil immersion) objective lens (Olympus). To avoid crosstalk between multiple fluorophores, Alexa Fluor-488 (or FITC), Cy3, and Cy5 fluorescent signals were acquired sequentially using the 488, 543, and 633 nm excitation laser lines, respectively. Single optical sections were obtained for low-powered images. (640 x 640 pixels; pixel size, 110 nm). To trace the morphology of immunolabeled LCs, z axis-stacked images were taken with 40x or 60x objective lens (8-10 optical slices at an interval of 1 μm). To obtain high-resolution images of the whole brain or cerebellum, micrographs were taken as segmented images and stuck together using a fluorescent microscope (BZ-X710, Keyence) equipped with a CFI Plan Apo λ (20x/0.20) objective lens.

Cerebellar compartment

Cerebellar compartments were visualized by immunolabeling for aldolase C. Using mid-sagittal cerebellar sections, the mean gray density of YC(+) elements was measured from

aldolase C(+) and aldolase C(-) stripes and from the border region, which was defined by < 20 μm from the border between zones (Fig. 6C). To assess PC input to LCs, calbindin(+)/aldolaseC(+) PC terminals on YC(+) LCs in the aldolaseC(+) stripe and calbindin(+)/aldolaseC(-) PC terminals on those in the aldolaseC(-) stripe were counted as matched contact (i.e., presumably input from PCs in the same compartment), while calbindin(+)/aldolaseC(+) PC terminals on those in the aldolaseC(-) stripe and calbindin(+)/aldolaseC(-) PC terminals on those in the aldolaseC(+) stripe were as mismatched contact (input from PCs beyond the compartment) (Fig. 6K). Images were analyzed with a Metamorph software (Universal Imaging Corp.). In all statistical analysis, data are represented as mean ± SEM. Samples are collected from three or four adult mice (postnatal day 30).

Immunoelectron microscopy

For double-labeling preembedding immunogold microscopy, microslicer sections were incubated with 0.1% sodium borohydride in 0.1% Tween 20-containing PBS for 10 min. After incubation with blocking solution (Aurion) for 30 min, sections were incubated overnight with a mixture of primary antibodies (GFP antibody in combination with VGluT1, VGluT2 or calbindin antibody, 1 μg/ml each) diluted with PBS containing 1% bovine serum albumin and 0.004% saponin, and incubated with 1.4 nm gold-conjugated secondary antibody (1:200; Nanogold; Nanoprobes) for 3 h. After intensive washing in 0.004% saponin/PBS, sections were treated with 2% glutaraldehyde in PB for 60 min and incubated with silver enhancement solution (SE-EM, Aurion) for 90 min. Sections were successively incubated with biotin-labeled secondary antibody (Jackson ImmunoResearch) for 2 sec and peroxidase-conjugated streptavidin (Nichirei) for 30 min.

The immunoreaction of avidin-biotin complex was visualized with 3,3'-diaminobenzidine (DAB). In single labeling, silver-enhanced immunogold microscopy was performed using GFP antibody. Sections were treated with 1% osmium tetroxide for 15 min, dehydrated, and embedded in Epon812 for the preparation of ultrathin sections (70 nm) using an Ultracut ultramicrotome (Leica).

Anterograde tracer labeling

CFs were selectively visualized by injecting 0.5 μl of 10% biotinylated dextran amine (BDA; 10,000 molecular weight; Invitrogen) or dextran Alexa 594 (DA594, Invitrogen) in PBS to the inferior olive by the dorsal approach (Miyazaki and Watanabe, 2011). A tracer-filled glass pipette was set on a stereotaxic unit with a manipulator (SR-5M, Narishige) at an angle of 58 degrees to the perpendicular line and at a pivot angle of 2 degrees lateral to the sagittal line, and was inserted to the medulla oblongata 1.0 mm lateral from the midline, 1.5 mm caudal from caudal edge of the occipital bone and 1.6 mm deep from the surface of the medulla. Tracer was injected by air pressure at 20 psi and at 5 sec intervals for 1 min (Pneumatic Picopump; World Precision Instruments). MFs were also labeled by injecting tracers into the lateral reticular nucleus (Zhan and Ryugo, 2007). For multiple fluorescent labeling, DA594-labeled microslicer sections were immunolabeled for calbindin, VGluT2 and GFP. Images of triple or quadruple labeling were taken with a FV1200 confocal microscope. For preembedding immunoelectron microscopy, BDA-labeled microslicer sections were processed for immunogold labeling for YC, in which BDA was visualized with DAB precipitates and YC was with silver-enhanced immunogold using GFP antibody. Sections were postfixed with 1% osmium tetroxide for 15 min, dehydrated in graded alcohols, and embedded in Epon 812.

Fluorescent* in situ *hybridization

For fluorescent *in situ* hybridization (FISH), cDNA fragments of mouse 67 kDa-glutamic acid decarboxylase (GAD67) (1036-2015 bp; GenBank, NM_008077), mouse GlyT2 (28-1154; AB118189.1), and mouse mGluR2 (194-1200; BC115866.1) were subcloned into the Bluescript II plasmid vector. Preparation of cRNA probes was performed as previously described (Yamasaki et al., 2010). Microslicer sections were treated with the following incubations: acetylation for 10 min with 0.25% acetic anhydride in 0.1 M triethanolamine-HCl, pH 8.0, and prehybridization for 1 h in a hybridization buffer (50% formamide, 50 mM Tris-HCl, pH 7.5, 0.02% Ficoll, 0.02% polyvinylpyrrolidone, 0.02% bovine serum albumin, 0.6 M NaCl, 200 μg/ml of tRNA, 1 mM EDTA, and 10% dextran sulfate). Hybridization was performed at 63.5 °C for 12 h in the hybridization buffer supplemented with cRNA probes at a dilution of 1:1000. Posthybridization washing was done at 61 °C successively with 5x SSC for 30 min, 4x SSC containing 50% formamide for 40 min, 2x SSC containing 50% formamide for 40 min, and 0.1x SSC for 30 min. Sections were dipped at room temperature in NTE buffer (0.5 M NaCl, 0.01 M Tris-HCl, pH 7.5, and 5 mM EDTA), 20 mM iodoacetamide in NTE buffer, and TNT buffer (0.1 M Tris-HCl pH 7.5, and 0.15 M NaCl) for 20 min each. Immunohistochemical detection of hybridized probes was done using FITC-TSA and Cy3-TSA plus amplification kits (PerkinElmer). Sections were subsequently immunolabeled for YC using GFP antibody.

In utero electroporation

For selective LC labeling, we performed *in utero* electroporation of DsRed. DsRed cDNA (GenBank FJ226078.1) was subcloned into the pCAGEN plasmid vector, a kind gift from Dr. Cepko (Addgene plasmid #11160 (Matsuda and Cepko, 2004). pCAGEN-DsRed

plasmid was purified using FastGene Xpress kit (Nippon Genetics), and dissolved in 10 mM Tris-HCl/1 mM EDTA (pH 8.0) at the final concentration of 1–5 mg/ml of Fast Green (final concentration 0.01%). Under pentobarbital anesthesia (50–60 mg/kg of body weight, i.p.) of pregnant D118-tTA::tetO-YC mice, the plasmid solution (1–3 μl) was injected into the fourth ventricle of embryos at embryonic day 14.5 (E14.5) by air pressure using a mouth-controlled micropipette. Embryos were held with tweezers-type electrodes through the uterus (CUY650P5; NEPA Gene), and electrical pulses (30 V, 30 ms duration at an intervals of 970 ms) were delivered five times using an electroporator (NEPA21; NEPA Gene). After suturing the peritoneum and skin, pups were born by normal delivery, and sacrificed at postnatal day 30 (P30).

Results

Characterization of YC(+) cells in D118-YC mice

We produced *Drd1*-tTA BAC transgenic mice, in which tTA is expressed under the promotor of dopamine receptor *Drd1* (Fig. 1A-C), and mated with tetO-YC knockin mice. Among ten founder lines of *Drd1*-tTA mice, the *Drd1*-tTA line 18 was found to induce YC expression in the cerebellum in addition to the cortex and the striatum, and referred to as D118-YC mice. (Fig. 1D). In the cerebellum of D118-YC mice, YC labeling appeared to be derived from distinct cell populations (Fig. 1E). Most typically, YC(+) cells had fusiform or flattened cell bodies lying just beneath the calbindin(+) PC layer, extended horizontal dendrites parallel to PC layer, and projected varicosed axons to the molecular layer (Fig. 1F, G). These cytological features are consistent with those of LCs

(Laine and Axelrad, 1996).

YC labeling was also found in the other cell types. At various depth of the granular layer, some YC(+) polygonal or spherical cells were located and extended dendrites radiating in the molecular layer (arrows in Fig. 1H). These cytological features likely represent Golgi cells, globular cells, or both. Because Golgi cells and globular cells project their axons to different cortical layers, i.e., the granular or molecular layer, respectively, and also because YC(+) axons were densely observed in the molecular layer, such YC(+) cells were likely to represent globular cells. This notion was supported by FISH for mGluR2, a Golgi cell marker (Simat et al., 2007); mGluR2 mRNA was rarely detected in YC(+) LCs (5.8 ± 1.9 % of YC(+) LCs; n=596 cells, 4 mice) (Fig. 2C). In rare cases, YC was detected in unipolar brush cells, an excitatory granular layer interneuron possessing a short dendritic brush (arrow in Fig. 1I*)* (Mugnaini et al., 2011) and detected in a few molecular layer interneurons (basket cells and stellate cells) and Bergmann glia that reside around PCs and extend radial fibers (Fig. 1J). Based on the above morphological classification, LCs were found to constitute 50.4 % of the total YC(+) cells in the D118-YC cerebellum (Fig. 1K; n=848 cells, 3 mice).

We also estimated the fraction of YC(+) cells in each cell type. Because most of the YC(+) cells that were located within 10 μm deep from the base of PC somata displayed typical LC morphology and expressed GAD67 mRNA (red and white arrowheads in Fig. 2A, B; n=346 cells, 4 mice), we tentatively classified GAD67 mRNA(+) cells in the superficial granular layer (< 10 μm from the bottom of the PC layer) or in the rest of the granular layer (> 10 μm) to be LCs or other granular layer interneurons, respectively. The fraction of YC(+) cells was estimated to be 36.2 ± 1.7 % (n =1002 cells, 4 mice) in the

total LC and 15.2 ± 4.8 % in the other granular layer interneurons (n=196 cells). We neurochemically identified the molecular layer interneuron as parvalbumin(+) cells in the molecular layer (Schneeberger et al., 1985), Bergmann glia as L-serine biosynthetic enzyme 3PGDH(+) cells in the PC layer (Furuya et al., 2000), and PCs as calbindin(+) cells. The fraction of YC(+) cells in the molecular layer interneuron, Bergmann glia, and PC was only 2.7 ± 0.5 % (n= 2050 cells), 2.6 ± 0.4 % (n=599 cells), and 5.0 ± 1.6 % (n=380 cells), respectively. Therefore, in the D118-YC cerebellum, nearly a half of YC(+) cells are LCs, and YC is expressed in one-third of the total LC population.

Neurochemical property

The neurochemical phenotype of YC(+) LCs was examined by FISH for GAD67 and GlyT2 mRNAs and immunofluorescence for YC (Fig. 2).We found that 62.6 ± 2.7 % of YC(+) LCs co-expressed GAD67 and GlyT2 mRNAs (red arrowheads in Fig. 2A), while 37.3 ± 2.7 % expressed GAD67 mRNA only (white arrowheads in Fig. 2B; red filled and open box plots in Fig. 2G, n=32 regions, 1002 cells, 4 mice). This suggests that two-thirds of YC(+) LCs are GABAergic/glycinergic, with most of the rest being exclusively GABAergic. CR has been used as a marker for LCs (Dieudonne and Dumoulin, 2000). CR was detected in 32.7 ± 4.2 % of YC(+) LCs and the rest of YC(+) LC (67.4 ± 4.2 %) were negative (n=27 regions, 331 cells, 4 mice) (Fig. 2D, E; yellow and green box plots in Fig. 2H). This indicates that CR is also expressed in one-third of YC(+) LCs.

Similar ratios of GlyT2(-) LCs and CR(+) LCs in YC(+) LCs (and vice versa) raised the possibility that they belong to the same population. To test this possibility, we conducted simultaneous labeling for GlyT2 mRNA and CR (Fig. 2F), and counted the

number of GlyT2(-)/CR(-), GlyT2(+)/CR(-), GlyT2(-)/CR(+), and GlyT2(+)/CR(+) cells in YC(+) LC populations (Fig, 2I, n=15 regions, 354 cells from 3 mice). Presence of GlyT2(-)/CR(-) and GlyT2(+)/CR(+) cell groups rejected the possibility. Nevertheless, higher ratios of GlyT2(-)/CR(+) and GlyT2(-)/CR(+) cell groups than GlyT2(-)/CR(-) and GlyT2(+)/CR(+) ones also showed that GlyT2 and CR expressions in YC(+) LCs tended to be negatively correlated.

Input source to LCs

We investigated the source of inputs to LCs by multiple fluorescent labeling. By triple immunolabeling for YC, calbindin, and vesicular glutamate transporter VGluT2, a marker for CF and MF terminals (Fig. 3A, B), fusiform somata and horizontal dendrites of YC(+) LCs were frequently contacted by calbindin(+) recurrent PC axons (green arrowheads, Fig. $3B_1$), and VGluT2(+) small (putative CF) and huge (putative MF) terminals (red arrows and arrowheads, respectively, Fig. $3B_2$). Innervation by CFs and MFs were confirmed by injecting anterograde tracer DA594 into their originating nuclei, i.e., the inferior olive and lateral reticular nucleus, respectively. DA594(+) CFs visualized small VGluT2(+) terminals attaching the soma and dendrites of YC(+) LCs (Fig. 3C, D), and DA594(+) MFs formed huge VGluT2(+) terminal rosettes on YC(+) LCs (Fig. 3E). Somatodendritic elements of YC(+) LCs were also contacted by terminals labeled for vesicular inhibitory amino acid transporter VIAAT (Fig. 3F), glycinergic fibers labeled for glycine transporter GlyT2 (Fig. 3G), small glutamatergic terminals labeled for VGluT1 (putative ascending axons of granule cells; Fig. 3H), and serotonergic fibers labeled for serotonin transporter HTT (Fig. 3I). Because glycinergic projections likely

arise from granular layer interneurons, such as Golgi cells and LCs (Laine and Axelrad, 2002; Ottersen et al., 1988; this study), we employed, to distinguish them, sparse neuronal labeling by *in utero* electroporation of DsRed to D118-YC mice at E14.5 (Fig. 3J, K). DsRed(+) Golgi cells were identified by large round or polygonal cell bodies located in the granular layer, rigid thick dendrites radiating in the molecular layer, and axonal arborization in the granular layer (Fig. 3J). Golgi cell axons contacted horizontal dendrites of YC(+) LCs. In case where DsRed was introduced into YC(+) LCs (yellow asterisk in Fig. 3K), YC(+)/DsRed(+) LC axons contacted dendrites of YC(+) LCs (arrows in inset of Fig. 3K). Thus, YC(+) LCs receive various inputs from CFs, MFs, granule cell axons, recurrent PC axons, Golgi cell axons, LC axons, and serotonergic fibers.

Inputs to YC(+) LCs were quantitated by measuring the number of contacted terminals and the length of analyzed somatic and dendritic surface (Fig. 3L-P; 3 mice). In this analysis, we identified excitatory inputs as VGluT1(+) or VGluT2(+) terminals (detected by mixture of VGluT1 and VGluT2 antibodies), and inhibitory inputs as VIAAT(+) terminals, respectively (Fig. 3M). We further classified inhibitory inputs from PCs and inhibitory interneurons as calbindin(+)/VIAAT(+) or calbindin(-)/VIAAT(+) terminals, respectively (Fig. 3N). As to excitatory inputs, CF and granule cell axon terminals were defined as small VGluT2(+) or VGluT1(+) terminals, respectively. MFs are known to form huge terminal rosettes, some of which express VGluT1 or VGluT2 alone and others express both (Nunzi et al., 2003). We thus identified MFs as huge terminals labeled for VGluT1 ,VGluT2, or both (Fig. 3O, P). Through this analysis, almost equal densities of inputs were noted at both soma and dendrites, with densities at dendritic portion being 2-3 times higher than those at somatic portion for each input (Fig.

3L). Two-dimensional scatter plots further showed positive and negative correlations between some inputs at both soma and dendrites of YC(+) LCs (Fig. 3M-P, Table 2). Positive correlation was observed between excitatory and inhibitory inputs (Fig. 3M), and also between CFs and granule cell axons (Fig. 3P). In contrast, negative correlation was found between PC and granular layer interneuron terminals (Fig. 3N) and between CF and MF terminals (Fig. 3O).

We examined junctional specializations between the above inputs and LCs by double-labeling preembedding immunoelectron microscopy for YC (labeled by metal particles) and for neurochemical markers or anterograde tracer BDA (labeled by diffuse DAB precipitates). As expected, calbindin(+) PC axons formed symmetrical synapses (Fig. 4A, B, white arrowheads), while BDA-labeled MFs (Fig. 4C, D) and CFs (Fig. 4E, F) formed asymmetrical synapses (black arrowheads) on YC(+) LCs. Small VGluT1(+) terminals also formed asymmetrical synapses on to LC dendrites (Fig. 4G, H); from perpendicular trajectory of VGluT1(+) axons in the granular layer, they were likely the ascending branch of T-shaped granule cell axons. GlyT2(+) terminals formed symmetrical synaptic contact onto YC(+) dendrites (Fig. 4I, J). YC(+)/VIAAT(+) (Fig. 4K, L) or YC(+)/GlyT2(+) (Fig. 4M, N) LC terminals also formed symmetrical synapses on YC(+) LC dendrites. Although HTT(+) serotonergic fibers intimately apposed LC dendrites for considerable distances, synapse-like specializations were hardly observed between them (Fig. 4O, P). Thus, LCs receive GABAergic and glycinergic inputs at symmetrical synapses and glutamatergic inputs at asymmetrical synapses. Serotonergic fibers, though intimately contact LC dendrites, form no conventional synapses.

Target of LC outputs

To trace the trajectory of LC axons, we analyzed D118-YC cerebella at P30, to which DsRed plasmid had been sparsely introduced at E14.5 by *in utero* electroporation (Fig. 5A-C). In horizontal cerebellar sections, DsRed(+)/YC(+) LC axons, which were emitted from dendrites of LCs (Fig. 5A, arrow; Fig. 5C, arrowheads), ascended to the molecular layer (*Aa* in Fig. 5A) and descended to the deep granular layer. In the molecular layer, DsRed(+)/YC(+) LC axons bifurcated into transverse axons (*Ta* in Fig. 5A), which further emitted ascending axons on the way. As a whole, YC(+) LC axons formed a dense lattice of axonal projection covering the entire molecular layer. Transverse axons ran long (> 1 mm) in the transverse plane, i.e., in the direction parallel to PF trajectory, extended beyond several borders between alternating aldolase C(+) and aldolase C(-) cerebellar stripes (Fig. 5A).

Neurochemical property of YC(+) LC axons was examined by double immunofluorescence for YC and VIAAT or GlyT2. All varicosities of YC(+) LC axons were VIAAT(+) (Fig. 5D). Some YC(+) LC axons were also intense for GlyT2 immunolabeling, whereas others were faint or negative (Fig. 5E). This is consistent with FISH data (Fig. 2F), thus indicating LCs to be inhibitory neurons consisting of dually GABAergic/glycinergic and singly GABAergic subsets.

Terminal varicosities of ascending and transverse LC axons frequently contacted somatodendritic elements of parvalbumin(+)/calbindin(-) molecular layer interneurons (asterisks in Fig. 5F-H). Of note, ascending LC axons profusely innervated individual molecular layer interneurons by attaching a series of terminal boutons on to somatodendritic elements of each target, while transverse axons contacted each target by

one or two terminals only (Fig. 5G). In contrast, somatodendritic elements of parvalbumin(+)/calbindin(+) PCs were densely innervated by parvalbumin(+)/calbindin(-) axons of molecular layer interneurons, but not by YC(+) LC axons (Fig. 5F). Neurogranin-labeled Golgi cell dendrites were densely innervated by ascending and transverse axons of LCs (Fig. 5I), consistent with an image showing dense innervation of DsRed(+) Golgi cell dendrites and soma by YC(+) LC axons (Fig. 3J). At the electron microscopic level, ascending (Fig. 5J, K) and transverse (Fig. 5 L-N) axons of YC(+) LCs formed symmetrical synapses with aspiny dendrites and soma of putative molecular layer interneurons and Golgi cells. Double-labeling preembedding immunoelectron microscopy confirmed that YC(+) LC terminals formed symmetrical synapses with neurogranin-labeled Golgi cell dendrites in the molecular layer (Fig. 5O, P). No synaptic contacts were found between YC(+) LC axons and spiny dendrites of PCs (data not shown).

Together, LCs send dually GABAergic/glycinergic or singly GABAergic inhibitory outputs to somatodendritic elements of molecular layer interneurons and Golgi cells, but not PCs, via their ascending and transverse axon branches.

Compartmentalized organization of LC dendrites

Longitudinally-oriented compartmentalization across cerebellar lobules is the fundamental organization of the cerebellar cortex (Apps and Hawkes, 2009). This organization is manifested as longitudinal stripes by banded patterns of molecular expression in PCs, such as aldolase C, and also as cerebellar zones and microzones by topographical projections of CFs from the inferior olive to the cerebellar cortex

(Andersson and Oscarsson, 1978; Brodal and Kawamura, 1980; Sugihara and Shinoda, 2004). Then we examined how LC dendrites were organized in relation with aldolase C stripes by triple immunofluorescence for YC (green or gray), calbindin (blue) and aldolase C (red) (Fig. 6A, B). Dendrites of LCs were extended in all directions, but more elongated to the rostrocaudal direction than to the transverse direction in both anterior (lobule 4/5, Fig. 6A) and posterior lobules (lobule 9, Fig. 6B). LC dendrites contacted neighboring ones, forming interconnected somatodendritic meshwork. Dendrodendritic and dendrosomatic contacts are confirmed by light and electron microscopic levels. Double labeling for YC and DsRed to DsRed-introduced LCs revealed close association and contact between neighboring LCs (Fig. 6C). Preembedding immunogold for YC demonstrated that apposed plasma membranes of two YC(+) LC dendrites were attached by adherens junctions having symmetrical condensations on both sides (White arrowheads in Fig. 6D).

When alternate zones by aldolase C(+)/calbindin(+) PCs (purple somata between dotted lines in Fig. 6A, B) and aldolaseC(-)/calbindin(+) PCs (blue) were overlaid, patterns of somatodendritic meshwork appeared to change or switch at the border of aldolase C zones (Fig. 6A, B). Consistent with this notion, the mean gray density of YC(+) elements in aldolase C(+) cerebellar zone (195.3 ± 12.7, n = 21 regions, 4 mice, Fig. 6E, red open column) and aldolase C(-) zone (190.3 ± 14.3, n = 46 regions, 4 mice, blue open column) stripes was similar to each other, but significantly higher than that in the border regions (< 20 μm from the border between zones) (110.2 ± 14.0; pink filled column, n = 62 regions, 4 mice, $p = 0.01166$ and $p = 0.03656$ in comparison with aldolase C(+) and (-) zones, respectively, Kruskal Wallis test). This raises the possibility that LC dendrites

are also compartmentalized according to aldolase C zones.

To address the zonal organization of LC dendrites, we employed single LC labeling by sparse *in utero* electroporation of DsRed. DsRed(+)/YC(+) LC dendrites were mainly arborized within single zones (Fig. 6F, G). We measured the total length of DsRed(+)/YC(+) LC dendrites inside the host zone (*inside*; white arrowheads in Fig. 6G*)* and those crossing the border into neighboring zones (*crossed*; black arrowheads). The length ratio of LC dendrites was 97.1 ± 1.1 % for the inside type and 2.9 ± 1.1 % for the crossed type ($p = 3.8\text{x}10^{-7}$, Student's *t*-test; n=48 regions, 48 cells and 199 dendrites from 3 mice, 11822.4 μm in total length of measured dendrites) (Fig. 6H). Thus, the majority of LC dendrites are arborized within a single aldolase C zone.

The fact that most (about 90%) of recurrent axon collaterals of PCs terminate in the same aldolase C zone in which the PC soma is located (Hawkes and Leclerc, 1989; Sugihara et al., 2009) suggests that LCs are likely to be innervated by PCs in the same aldolase C zone. Finally, we tested this by triple immunofluorescence for calbindin, YC, and aldolase C (Fig. 6I, J). As expected, YC(+) LCs in aldolase C(-) zone (asterisk in Fig. 6I, J) were contacted by many calbindin(+)/aldolase C(-) PC terminals and a few calbindin(+)/aldolase C(+) ones (Fig. 6J), and vice versa. The density of neurochemically-matched PC terminals on YC(+) LC soma and dendrites (0.110 ± 0.005/μm) was significantly higher than that of neurochemically-mismatched ones (0.018 ± 0.002/μm) (Fig. 6K, $p<1.0\text{x}10^{-10,}$ Mann-Whitney *U*-test; n=299 dendrites form 3 mice, 21379.3 μm in total measured length). Taken together, LC circuits are also subjected to cerebellar compartments, at least, through compartmentalized arborization of LC dendrites and exclusive inputs from PCs within a given compartment.

Discussion

Using the D118-YC mouse line, we characterized neurochemical and input-output organizations of YC(+) LCs and further clarified their relationships with cerebellar compartments (Fig. 7A).

D118-YC mouse

In the D118-YC cerebellum, YC is neither selective to LCs nor expressed in all LCs. Compared with GAD67/GFP mice that label all GABAergic neurons, including LCs (Hirono et al., 2012), D118-YC mice were a useful animal model to study basic morphological properties of LCs. So far, immunohistochemistry with CR and cell-specific monoclonal antibodies has been used to analyze LC cytology. These antibodies label the soma and proximal shaft dendrites (i.e., cytoplasm-rich portions) strongly, but peripheral thin processes weakly or negatively, thus hampering full-extent visualization of single neuron morphology (Rogers, 1989; Sahin and Hockfield, 1990; Arai et al., 1991). Golgi-impregnated method is suited for this purpose, but impregnated neurons are limited in further characterization by combination with other histochemical analyses (Laine and Axelrad, 2002). YC expression in D118-YC mice is high enough to thoroughly follow individual dendrites and axons at both the light and electron microscopic levels. Direct fluorescence would enable electrophysiological approach to LCs and ratiometric Ca^{2+} imaging in LCs *in vivo,* as has been applied to YC-expressing astrocytes in the somatosensory cortex (Kanemaru et al., 2014). Furthermore, the application of the

intersectional targeting with Cre/tTA-dependent reporter lines can narrow gene induction in LCs, for example, CR-Cre; *Drd1*-tTA line 18; Ai93 (TITL-GCaMP6f) triple transgenic mice that express GCaMP6f only in CR-positive LCs (Taniguchi et al., 2011; Madisen et al., 2015).

In situ hybridization failed to detect *Drd1* mRNA in the wild-type cerebellum, and 9 out of 10 *Drd1*-tTA founders did not induce YC expression in LCs after crossing to tetO-YC knockin mice (our unpublished data). These findings suggest that YC expression in LCs is entirely ectopic in D118-YC mice and *Drd1* promoter is inactive in native LCs. We assume that serendipitous combination of the chromosomal positional effect on the transgene and the *Drd1* promoter activity in BAC clone may produce the transcriptional activity in LCs of D118-YC mice.

Neurochemical property

We showed that 63% of YC(+) LCs expressed both GAD67 and GlyT2 mRNAs. The presence of GABAergic/glycinergic LCs is consistent with previous histochemical studies (Takayama, 1994; Dumoulin et al., 2001; Simat et al., 2007), and also with an electrophysiological study showing that inhibitory postsynaptic currents (IPSCs) at LC-Golgi cell synapses are mediated by $GABA_A$ and glycine receptors (Dumoulin et al., 2001). We also showed that 31% of YC(+) LCs were singly GABAergic. Such a mixed neurochemical composition has been reported for Golgi cells (Wilkin et al., 1981), where 71%, 14%, and 14% are immunolabeled for GABA and glycine, GABA only, and glycine only, respectively (Ottersen et al., 1988). Taking purely GABAergic phenotype in basket and stellate cells (Gabbott et al., 1986; Ottersen et al., 1988; Dumoulin et al., 2001),

neurochemical heterogeneity is common to inhibitory interneurons in the granular layer, and likely reflects their cellular diversity.

In our estimate, a half of YC(+) cells were LCs, and YC was expressed in one-third of the total LC population. Among YC(+) LCs, all four combination patterns of GlyT2 and CR expressions were discerned. These findings support the heterogeneity in gene expression profiles among LC populations, and further studies are needed to determine whether qualitative and quantitative characteristics revealed from YC(+) LCs are applicable to the whole LC population.

LC input

Early electron microscopic studies described that LCs are innervated exclusively (95%) by recurrent PC axons and sparsely (5%) by granule cell axons (Lemkey-Johnston and Larramendi, 1968). In contrast to the limited input sources, the present study has disclosed various inputs to LCs (Fig. 7A). Novel inputs hitherto unknown include CFs, MFs, LC axons, Golgi cell axons, and serotonergic fibers. Moreover, we could disclose that LCs received these inputs at similar densities, showing some positive and negative correlations. Positive correlation in densities between excitatory and inhibitory inputs may reflect the excitatory/inhibitory balance in LCs. Negative correlation in input densities between PCs and granular layer interneurons and between CFs and MFs might imply their competitive nature in synaptogenesis.

The wealth of LC inputs is an important finding in this study, and relevant to previous functional studies. Conjunctive activation of CFs and peripheral sensory afferents (i.e., MFs) causes long-lasting depression of Golgi cell firing (Schulman and

Bloom, 1981; Xu and Edgley, 2008). CFs emit thin branches named Sheibel collaterals, which enter the PC and granular layers (Scheibel and Scheibel, 1954; Sugihara et al., 1999). Although Sheibel collaterals approach the soma and dendrite of Golgi cells (Hámori and Szentágothai, 1966; Shinoda et al., 2000), their synaptic contact with Golgi cells fails to be captured so far (Galliano et al., 2013). Considering converging CF and MF inputs to LCs and LC outputs to Golgi cells, it is possible to assume that conjunctive activities of CFs and MFs induce LC firing, which in turn inhibits Golgi cell firing.

Another relevance is serotonergic wiring to LCs. LCs are normally quiescent, but robustly fire in the presence of serotonin, leading to long-range inhibition of molecular layer interneurons and Golgi cells and to the generation of oscillatory IPSCs in Golgi cells (Dieudonne and Dumoulin, 2000; Hirono et al., 2012). LCs themselves or inputs to LCs are likely the primary target of serotonergic modulation (Dieudonne and Dumoulin, 2000; Hirono et al., 2012). Moreover, serotonin level in the cerebellar cortex is positively correlated to the level of motor activity of the animal (Mendlin et al., 1996). We showed anatomical evidence for intimate association of serotonergic fibers with LC soma and dendrites without forming synaptic specialization. This suggests that serotonergic fibers are preferentially anchored to LCs to let them release serotonin at the very vicinity of LCs. This could be the molecular-anatomical basis, at least partly, for potent and preferential serotonergic modulation of LCs.

LC output

We could demonstrate the anatomical organization of ascending and transverse LC axons, and they innervated molecular layer interneurons, Golgi cells, but not PCs. These findings

are fully consistent with previous studies (Laine and Axelrad, 1996, 1998; Dieudonne and Dumoulin, 2000; Dumoulin et al., 2001; Laine and Axelrad, 2002). Furthermore, we could demonstrate LC-LC interconnection via axodendritic symmetrical synapses and dendrodendritic adherens junctions.

Both branch types of LC axons constructed a dense lattice casting to the entire molecular layer (Fig. 5A). Of note, ascending axons profusely innervated given targets by attaching them with multiple terminal boutons, while transverse axons contacted given targets with one or two terminals only. This orthogonal projection system resembles that by CFs and PFs on to PC dendrites. This suggests that ascending LC axons can cast strong inhibition to particular targets, like CFs, while transverse LC axons may convey weak inhibition to numerous targets, like PFs.

Cerebellar compartment

The cerebellar cortex is parasagittally compartmentalized by topographical projections of cerebellar afferents and efferents (Apps and Hawkes, 2009). Such compartmentalization is known for projections of CFs to PCs (Brodal and Kawamura, 1980; Sugihara and Shinoda, 2004, 2007; Reeber et al., 2012; Fujita and Sugihara, 2013), MFs to granule cells (Sillitoe et al., 2003; Gebre et al., 2012), recurrent PC axons to PCs, molecular layer interneurons, and LCs (Sugihara et al., 2009; Witter et al., 2016), and PC axons to the cerebellar and vestibular nuclei (Apps and Hawkes, 2009). Local wiring by cerebellar interneurons is also subjected to compartmentalized restriction (Consalez and Hawkes, 2013). As with PCs, dendrites of molecular layer interneurons and Golgi cells are arborized in the parasagittal plane, and thereby confined to given cerebellar compartments

(Hawkes and Leclerc, 1989; Gao et al., 2006; Sillitoe et al., 2008; Consalez and Hawkes, 2012). Axons of molecular layer interneurons also project in the parasagittal plane and their inhibitory fields are confined to given compartments (Jorntell et al., 2010).

Another important finding in the present study is that the LC is one such interneuron conforming to the cerebellar compartmentalization, as shown by preferential dendritic arborization (Fig. 6H) and PC-LC innervation (Fig. 6K) within given compartments. This indicates that excitatory, inhibitory, and modulatory inputs to LCs are processed and integrated in compartments that they belong to. Then, LCs send inhibitory outputs to molecular layer interneurons and Golgi cells. Taking dense target innervation by ascending LC axons, it can be assumed that LCs can strongly inhibit molecular layer interneurons and Golgi cells in the same compartment. When LC activities are elevated, LC-mediated inhibition may propagate beyond the compartment through sparse long-range innervation by transverse LC axons. Thus, LCs integrate various compartmentalized cerebellar inputs and send inhibitory outputs mainly to the belonging compartment, and can also influence the neighboring compartments.

Functional implication

Basket cells project axons to as many as 50-70 PCs (Eccles et al., 1967). In response to PF or CF activities, basket cells can cause synchronous pause of PC spikes within a compartment (Mittmann et al., 2005; Bao et al., 2010; Mathews et al., 2012; Coddington et al., 2013). Recurrent connections between PCs also play an important role in synchronous PC activities (de Solages et al., 2008), and are essential for time-locked spiking in the cerebellar nuclei (Person and Raman, 2012) and motor learning (Wulff et

al., 2009). On the other hand, Golgi cells act as a filter of synchronous MF activities on to granule cells through feed-forward inhibition via the Golgi cell-granule cell pathway and also through feed-back inhibition via the granule cell-PF-Golgi cell-granule cell loop (Fig.7B, right) (Kanichay and Silver, 2008). Accordingly, as a unique interneuron-targeting interneuron, LCs could effectively modulate cerebellar cortical activities through disinhibition of PCs via LC-mediated inhibition of molecular layer interneurons (Fig. 7B, left) and also through disinhibition of granule cells via LC-mediated inhibition of Golgi cells (right). Furthermore, this configuration of LC circuits might be the strategic node of serotonergic modulation of cerebellar cortical activities. Functional relevance of these anatomical notions needs to be challenged in future studies.

References

Andersson G, Oscarsson O (1978) Climbing fiber microzones in cerebellar vermis and their projection to different groups of cells in the lateral vestibular nucleus. Experimental brain research 32:565-579.

Apps R, Hawkes R (2009) Cerebellar cortical organization: a one-map hypothesis. Nat Rev Neurosci 10:670-681.

Arai R, Winsky L, Arai M, Jacobowitz DM (1991) Immunohistochemical localization of calretinin in the rat hindbrain. J Comp Neurol 310:21-44.

Bao J, Reim K, Sakaba T (2010) Target-dependent feedforward inhibition mediated by short-term synaptic plasticity in the cerebellum. J Neurosci 30:8171-8179.

Blot A, Barbour B (2014) Ultra-rapid axon-axon ephaptic inhibition of cerebellar Purkinje cells by the pinceau. Nat Neurosci 17:289-295.

Bower JM (2010) Model-founded explorations of the roles of molecular layer inhibition in regulating purkinje cell responses in cerebellar cortex: more trouble for the beam hypothesis. Front Cell Neurosci 4.

Brodal A, Kawamura K (1980) Olivocerebellar projection: a review. Adv Anat Embryol Cell Biol 64:Iviii, 1-140.

Coddington LT, Rudolph S, Vande Lune P, Overstreet-Wadiche L, Wadiche JI (2013) Spillover-mediated feedforward inhibition functionally segregates interneuron activity. Neuron 78:1050-1062.

Consalez GG, Hawkes R (2012) The compartmental restriction of cerebellar interneurons. Front Neural Circuits 6:123.

Consalez GG, Hawkes R (2013) The compartmental restriction of cerebellar interneurons. Front Neural Circuits 6:123.

de Solages C, Szapiro G, Brunel N, Hakim V, Isope P, Buisseret P, Rousseau C, Barbour B, Lena C (2008) High-frequency organization and synchrony of activity in the purkinje cell layer of the cerebellum. Neuron 58:775-788.

Dieudonne S, Dumoulin A (2000) Serotonin-driven long-range inhibitory connections in the cerebellar cortex. J Neurosci 20:1837-1848.

Dumoulin A, Triller A, Dieudonne S (2001) IPSC kinetics at identified GABAergic and mixed GABAergic and glycinergic synapses onto cerebellar Golgi cells. J Neurosci 21:6045-6057.

Eccles JC, Ito M, Szentágothai J (1967) The Cerebellum as a Neuronal Machine. Berlin:Springer-Verlag.

Eyre MD, Nusser Z (2016) Only a Minority of the Inhibitory Inputs to Cerebellar Golgi Cells Originates from Local GABAergic Cells. eNeuro 3.

Floris A, Dino M, Jacobowitz DM, Mugnaini E (1994) The unipolar brush cells of the rat cerebellar cortex and cochlear nucleus are calretinin-positive: a study by light and electron microscopic immunocytochemistry. Anat Embryol (Berl) 189:495-520.

Fujita H, Sugihara I (2013) Branching patterns of olivocerebellar axons in relation to the compartmental organization of the cerebellum. Front Neural Circuits 7:3.

Fukaya M, Tsujita M, Yamazaki M, Kushiya E, Abe M, Akashi K, Natsume R, Kano M, Kamiya H, Watanabe M, Sakimura K (2006) Abundant distribution of TARP gamma-8 in synaptic and extrasynaptic surface of hippocampal neurons and its major role in AMPA receptor expression on spines and dendrites. The European journal of neuroscience 24:2177-2190.

Fukudome Y, Ohno-Shosaku T, Matsui M, Omori Y, Fukaya M, Tsubokawa H, Taketo MM, Watanabe M, Manabe T, Kano M (2004) Two distinct classes of muscarinic

action on hippocampal inhibitory synapses: M2-mediated direct suppression and M1/M3-mediated indirect suppression through endocannabinoid signalling. The European journal of neuroscience 19:2682-2692.

Furuya S, Tabata T, Mitoma J, Yamada K, Yamasaki M, Makino A, Yamamoto T, Watanabe M, Kano M, Hirabayashi Y (2000) L-serine and glycine serve as major astroglia-derived trophic factors for cerebellar Purkinje neurons. Proceedings of the National Academy of Sciences 97:11528-11533.

Gabbott PL, Somogyi J, Stewart MG, Hamori J (1986) GABA-immunoreactive neurons in the rat cerebellum: a light and electron microscope study. J Comp Neurol 251:474-490.

Galliano E, Baratella M, Sgritta M, Ruigrok TJ, Haasdijk ED, Hoebeek FE, D'Angelo E, Jaarsma D, De Zeeuw CI (2013) Anatomical investigation of potential contacts between climbing fibers and cerebellar Golgi cells in the mouse. Front Neural Circuits 7:59.

Gao W, Chen G, Reinert KC, Ebner TJ (2006) Cerebellar cortical molecular layer inhibition is organized in parasagittal zones. J Neurosci 26:8377-8387.

Gebre SA, Reeber SL, Sillitoe RV (2012) Parasagittal compartmentation of cerebellar mossy fibers as revealed by the patterned expression of vesicular glutamate transporters VGLUT1 and VGLUT2. Brain Struct Funct 217:165-180.

Golgi C (1879) Di una nuova reazione apparentemente nera delle cellule nervose cerebrali ottenuta col bicloruro di mercurio. Arch Sci Med 3:1-7.

Hámori J, Szentágothai J (1966) Identification under the electron microscope of climbing fibers and their synaptic contacts. Experimental Brain Research 1:65-81.

Hawkes R, Leclerc N (1989) Purkinje cell axon collateral distributions reflect the

chemical compartmentation of the rat cerebellar cortex. Brain Res 476:279-290.

Hirono M, Saitow F, Kudo M, Suzuki H, Yanagawa Y, Yamada M, Nagao S, Konishi S, Obata K (2012) Cerebellar globular cells receive monoaminergic excitation and monosynaptic inhibition from Purkinje cells. PloS one 7:e29663.

Hondo M, Furutani N, Yamasaki M, Watanabe M, Sakurai T (2011) Orexin neurons receive glycinergic innervations. PloS one 6:e25076.

Ichikawa R, Yamasaki M, Miyazaki T, Konno K, Hashimoto K, Tatsumi H, Inoue Y, Kano M, Watanabe M (2011) Developmental switching of perisomatic innervation from climbing fibers to basket cell fibers in cerebellar Purkinje cells. J Neurosci 31:16916-16927.

Ito M, Yamaguchi K, Nagao S, Yamazaki T (2014) Long-term depression as a model of cerebellar plasticity. Progress in brain research 210:1-30.

Iwakura A, Uchigashima M, Miyazaki T, Yamasaki M, Watanabe M (2012) Lack of molecular-anatomical evidence for GABAergic influence on axon initial segment of cerebellar Purkinje cells by the pinceau formation. J Neurosci 32:9438-9448.

Jorntell H, Bengtsson F, Schonewille M, De Zeeuw CI (2010) Cerebellar molecular layer interneurons - computational properties and roles in learning. Trends Neurosci 33:524-532.

Kanemaru K, Sekiya H, Xu M, Satoh K, Kitajima N, Yoshida K, Okubo Y, Sasaki T, Moritoh S, Hasuwa H, Mimura M, Horikawa K, Matsui K, Nagai T, Iino M, Tanaka KF (2014) In vivo visualization of subtle, transient, and local activity of astrocytes using an ultrasensitive Ca(2+) indicator. Cell Rep 8:311-318.

Kanichay RT, Silver RA (2008) Synaptic and cellular properties of the feedforward inhibitory circuit within the input layer of the cerebellar cortex. J Neurosci

28:8955-8967.

Kano M, Watanabe M (2013) Cerebellar circuits. In: Comprehensive Developmental Neuroscience: Neural Circuit Development and Function in the Healthy and Diseased Brain. Elsevier, Amsterdam volume 3.

Korn H, Axelrad H (1980) Electrical inhibition of Purkinje cells in the cerebellum of the rat. Proc Natl Acad Sci U S A 77:6244-6247.

Kurihara H, Hashimoto K, Kano M, Takayama C, Sakimura K, Mishina M, Inoue Y, Watanabe M (1997) Impaired parallel fiber-->Purkinje cell synapse stabilization during cerebellar development of mutant mice lacking the glutamate receptor delta2 subunit. J Neurosci 17:9613-9623.

Laine J, Axelrad H (1996) Morphology of the Golgi-impregnated Lugaro cell in the rat cerebellar cortex: a reappraisal with a description of its axon. J Comp Neurol 375:618-640.

Laine J, Axelrad H (1998) Lugaro cells target basket and stellate cells in the cerebellar cortex. Neuroreport 9:2399-2403.

Laine J, Axelrad H (2002) Extending the cerebellar Lugaro cell class. Neuroscience 115:363-374.

Lemkey-Johnston N, Larramendi LM (1968) Types and distribution of synapses upon basket and stellate cells of the mouse cerebellum: an electron microscopic study. J Comp Neurol 134:73-112.

Lugaro E (1894) Sulle connessioni tra gli elementi nervosi della corteccia cerebellare con considerazioni generali sul significato fisiologico dei rapporti tra gli elementi nervosi. Rivista Sperimentale di Freniatria 20:297-331.

Madisen L et al. (2015) Transgenic mice for intersectional targeting of neural sensors and

effectors with high specificity and performance. Neuron 85:942-958.

Mathews PJ, Lee KH, Peng Z, Houser CR, Otis TS (2012) Effects of climbing fiber driven inhibition on Purkinje neuron spiking. J Neurosci 32:17988-17997.

Matsuda T, Cepko CL (2004) Electroporation and RNA interference in the rodent retina in vivo and in vitro. Proc Natl Acad Sci U S A 101:16-22.

Mendlin A, Martín FJ, Rueter LE, Jacobs BL (1996) Neuronal release of serotonin in the cerebellum of behaving rats: an in vivo microdialysis study. Journal of neurochemistry 67:617-622.

Mittmann W, Koch U, Hausser M (2005) Feed-forward inhibition shapes the spike output of cerebellar Purkinje cells. J Physiol 563:369-378.

Miyazaki T, Watanabe M (2011) Development of an anatomical technique for visualizing the mode of climbing fiber innervation in Purkinje cells and its application to mutant mice lacking GluRd2 and $Ca_V2.1$. Anat Sci Int 86:10-18.

Miyazaki T, Yamasaki M, Uchigashima M, Matsushima A, Watanabe M (2011) Cellular expression and subcellular localization of secretogranin II in the mouse hippocampus and cerebellum. The European journal of neuroscience 33:82-94.

Mugnaini E, Sekerkova G, Martina M (2011) The unipolar brush cell: a remarkable neuron finally receiving deserved attention. Brain Res Rev 66:220-245.

Nakamura M, Sato K, Fukaya M, Araishi K, Aiba A, Kano M, Watanabe M (2004) Signaling complex formation of phospholipase Cbeta4 with metabotropic glutamate receptor type 1alpha and 1,4,5-trisphosphate receptor at the perisynapse and endoplasmic reticulum in the mouse brain. The European journal of neuroscience 20:2929-2944.

Napper RM, Harvey RJ (1988) Number of parallel fiber synapses on an individual

Purkinje cell in the cerebellum of the rat. J Comp Neurol 274:168-177.

Nunzi MG, Russo M, Mugnaini E (2003) Vesicular glutamate transporters VGLUT1 and VGLUT2 define two subsets of unipolar brush cells in organotypic cultures of mouse vestibulocerebellum. Neuroscience 122:359-371.

Ottersen OP, Storm-Mathisen J, Somogyi P (1988) Colocalization of glycine-like and GABA-like immunoreactivities in Golgi cell terminals in the rat cerebellum: a postembedding light and electron microscopic study. Brain Res 450:342-353.

Palay S, Chan-Palay V (1974) Cerebellar cortex: Cytology and organization. New York: Springer:pp 63-69, 242-287.

Person AL, Raman IM (2012) Purkinje neuron synchrony elicits time-locked spiking in the cerebellar nuclei. Nature 481:502-505.

Reeber SL, White JJ, George-Jones NA, Sillitoe RV (2012) Architecture and development of olivocerebellar circuit topography. Front Neural Circuits 6:115.

Rogers JH (1989) Immunoreactivity for calretinin and other calcium-binding proteins in cerebellum. Neuroscience 31:711-721.

Sahin M, Hockfield S (1990) Molecular identification of the Lugaro cell in the cat cerebellar cortex. J Comp Neurol 301:575-584.

Scheibel ME, Scheibel AB (1954) Observations on the intracortical relations of the climbing fibers of the cerebellum; a Golgi study. J Comp Neurol 101:733-763.

Schneeberger P, Norman A, Heizmann C (1985) Parvalbumin and vitamin D-dependent calcium-binding protein (Mr 28,000): comparison of their localization in the cerebellum of normal and rachitic rats. Neuroscience letters 59:97-103.

Schulman JA, Bloom FE (1981) Golgi cells of the cerebellum are inhibited by inferior olive activity. Brain research 210:350-355.

Shinoda Y, Sugihara I, Wu HS, Sugiuchi Y (2000) The entire trajectory of single climbing and mossy fibers in the cerebellar nuclei and cortex. Progress in brain research 124:173-186.

Sillitoe RV, Benson MA, Blake DJ, Hawkes R (2003) Abnormal dysbindin expression in cerebellar mossy fiber synapses in the mdx mouse model of Duchenne muscular dystrophy. J Neurosci 23:6576-6585.

Sillitoe RV, Chung SH, Fritschy JM, Hoy M, Hawkes R (2008) Golgi cell dendrites are restricted by Purkinje cell stripe boundaries in the adult mouse cerebellar cortex. J Neurosci 28:2820-2826.

Simat M, Parpan F, Fritschy JM (2007) Heterogeneity of glycinergic and gabaergic interneurons in the granule cell layer of mouse cerebellum. J Comp Neurol 500:71-83.

Somogyi J, Baude A, Omori Y, Shimizu H, El Mestikawy S, Fukaya M, Shigemoto R, Watanabe M, Somogyi P (2004) GABAergic basket cells expressing cholecystokinin contain vesicular glutamate transporter type 3 (VGLUT3) in their synaptic terminals in hippocampus and isocortex of the rat. The European journal of neuroscience 19:552-569.

Sugihara I, Shinoda Y (2004) Molecular, topographic, and functional organization of the cerebellar cortex: a study with combined aldolase C and olivocerebellar labeling. J Neurosci 24:8771-8785.

Sugihara I, Shinoda Y (2007) Molecular, topographic, and functional organization of the cerebellar nuclei: analysis by three-dimensional mapping of the olivonuclear projection and aldolase C labeling. J Neurosci 27:9696-9710.

Sugihara I, Wu H, Shinoda Y (1999) Morphology of single olivocerebellar axons labeled

with biotinylated dextran amine in the rat. J Comp Neurol 414:131-148.

Sugihara I, Fujita H, Na J, Quy PN, Li BY, Ikeda D (2009) Projection of reconstructed single Purkinje cell axons in relation to the cortical and nuclear aldolase C compartments of the rat cerebellum. J Comp Neurol 512:282-304.

Szapiro G, Barbour B (2007) Multiple climbing fibers signal to molecular layer interneurons exclusively via glutamate spillover. Nat Neurosci 10:735-742.

Takasaki C, Yamasaki M, Uchigashima M, Konno K, Yanagawa Y, Watanabe M (2010) Cytochemical and cytological properties of perineuronal oligodendrocytes in the mouse cortex. The European journal of neuroscience 32:1326-1336.

Takayama C (1994) Altered distribution of inhibitory synaptic terminals in reeler cerebellum with special reference to malposition of GABAergic neurons. Neuroscience research 20:239-250.

Taniguchi H, He M, Wu P, Kim S, Paik R, Sugino K, Kvitsiani D, Fu Y, Lu J, Lin Y, Miyoshi G, Shima Y, Fishell G, Nelson SB, Huang ZJ (2011) A resource of Cre driver lines for genetic targeting of GABAergic neurons in cerebral cortex. Neuron 71:995-1013.

Watanabe D, Inokawa H, Hashimoto K, Suzuki N, Kano M, Shigemoto R, Hirano T, Toyama K, Kaneko S, Yokoi M, Moriyoshi K, Suzuki M, Kobayashi K, Nagatsu T, Kreitman RJ, Pastan I, Nakanishi S (1998) Ablation of cerebellar Golgi cells disrupts synaptic integration involving GABA inhibition and NMDA receptor activation in motor coordination. Cell 95:17-27.

Watanabe M (2016) Basket cells: In: Essentials of Cerebellum and Cerebellar Disorders (Eds. Gruol DL, Koibuchi N, Manto M, Molinari M, Schmahmann N, Shen Y), Springer.

Wilkin GP, Csillag A, Bala R, Kingsbury AE, Wilson JE, Johnson AL (1981) Localization of high affinity [3H] glycine transport sites in the cerebellar cortex. Brain research 216:11-33.

Witter L, Rudolph S, Pressler RT, Lahlaf SI, Regehr WG (2016) Purkinje Cell Collaterals Enable Output Signals from the Cerebellar Cortex to Feed Back to Purkinje Cells and Interneurons. Neuron 91:312-319.

Wulff P, Schonewille M, Renzi M, Viltono L, Sassoe-Pognetto M, Badura A, Gao Z, Hoebeek FE, van Dorp S, Wisden W, Farrant M, De Zeeuw CI (2009) Synaptic inhibition of Purkinje cells mediates consolidation of vestibulo-cerebellar motor learning. Nat Neurosci 12:1042-1049.

Xu W, Edgley S (2008) Climbing fibre‐dependent changes in Golgi cell responses to peripheral stimulation. The Journal of physiology 586:4951-4959.

Yamasaki M, Matsui M, Watanabe M (2010) Preferential localization of muscarinic M1 receptor on dendritic shaft and spine of cortical pyramidal cells and its anatomical evidence for volume transmission. J Neurosci 30:4408-4418.

Zhan X, Ryugo DK (2007) Projections of the lateral reticular nucleus to the cochlear nucleus in rats. J Comp Neurol 504:583-598.

Figure legend

Fig 1. YC expression in the brain and cerebellum of D118-YC mice. *A-C*. Generation of construct and tTA-mediated YC induction. *A*. Drd1 gene structure. *B*. Drd1-tTA construct. tTA-polyA cassette was inserted into the translation initiation site (ATG) in the exon 2 of Drd1 gene. *C*. YC induction in tTA-expressing cells in Drd1-tTA::tetO-YC double transgenic mice. *D-J*. Single immunofluorescence for YC (*D, E, G. H*) or double immunofluorescence for YC (green) and calbindin (red, *F, I, J*). *D, E*. Overall expression of YC in parasagittal sections of the adult brain (*D*) and cerebellum (*E*). The number of cerebellar lobules is indicated by numerals 1-10. *F, G*. YC(+) LCs. LCs place their somata just beneath the PC layer, extend horizontal dendrites (arrows), and project axons to the molecular layer (arrowheads). *H*. Putative YC(+) globular cell (GlC). *I*. YC(+) unipolar brush cell (UBC) and granular layer interneurons other than LCs (GLI). The former cell was identified by the presence of characteristic dendritic brush (arrow). *J*. YC(+) Bergmann glia (BG) and molecular layer interneuron (MLI). *K*. A pie chart graph showing the percentage of cell types in the total YC(+) cells in the cerebellar cortex. Cb, cerebellum; Cx, cerebral cortex; GL, granular layer; GP, globus pallidus; Hp, hippocampus; IC, inferior colliculus; ML, molecular layer; MO, medulla oblongata; OB, olfactory bulb; PL, Purkinje cell layer; SC, superior colliculus; SN, substantia nigra; Str, striatum. Scale bars, *D, E*, 1 mm; *F*, 50 μm; *G-J*, 20 μm.

Fig 2. Neurochemical properties of YC(+) LCs. *A, B*. Double FISH for GlyT2 (red or gray) and GAD67 (blue or gray) mRNAs combined with immunofluorescence for YC (green). Note that all of YC(+) LCs expressed GAD67 mRNA (red, and white

arrowheads). Of these, red arrows indicate a YC(+) LC expressing both GAD67 and GlyT2 mRNAs, while white arrowheads indicate a YC(+) LC expressing GAD67 mRNA alone. Some YC(-) neurons express both GAD67 and GlyT2 mRNAs beneath the PC layer (black arrowheads), confirming that not all LCs express YC. *C*. Single FISH for mGluR2 mRNA (red or gray) combined with immunofluorescence for YC (green). Note the lack of mGluR2 mRNA expression in a YC(+) LC (arrow). *D, E*. Double immunofluorescence for YC (green) and CR (Red or gray). Some YC(+) LC expressed CR (yellow asterisk) but more than two-thirds of YC(+) LC does not expressed CR (green asterisk). *F*. Immunofluorescence for YC (green) and CR (blue or gray) and FISH for GlyT2 mRNA (Red or gray). White and orange asterisks show GlyT2(-)/CR(-) and GlyT2(+)/CR(+)YC(+) LCs, respectively. *G*. Box plots showing the ratio of YC(+) LCs positive (red) or negative (white) to GlyT2 mRNA labeling. *H*. Box plots showing the ratio of YC(+) LCs positive (yellow) or negative (green) to CR labeling. *I.* Box plots showing the ratio of GlyT2(-)/CR(-) (white), GlyT2(+)/CR(-) (red), GlyT2(-)/CR(+) (yellow) and GlyT2(+)/CR(+) (orange) cells in YC(+) LC populations. All box plots display median, 25th and 75th percentiles and whisker boundaries indicate the 10th and 90th percentiles. Scale bars, 10 μm.

Fig 3. Immunofluorescence characterizing input sources to LCs. *A, B*. Triple immunofluorescence for YC (gray), calbindin (green), and VGluT2 (red). A boxed region of *A* is enlarged in *B*. Green arrowheads in B_1 indicate frequent contact of calbindin(+) recurrent PC axons on YC(+) LC soma and dendrites. Likewise, red arrowheads and arrows in B_2 indicate frequent contact of VGluT2(+) huge MF terminal rosettes or

VGluT2(+) small CF terminals on YC(+) LC dendrites. *C-E*. Triple fluorescent labeling for YC (gray), anterograde tracer DA594 (red), and VGluT2 (green). A boxed region of *C* is enlarged in *D*. YC(+) LC dendrites are contacted by small CF terminals labeled for VGluT2 and DA594 injected into the inferior olive (arrowheads, *D*), and also by large MF terminals labeled for VGluT2 and DA594 injected into the lateral reticular nucleus (arrows, *E*). *F-I*. Double immunofluorescence for YC (green) and neurochemical markers (red), including inhibitory terminal marker VIAAT (*F*), glycinergic fiber marker GlyT2 (*G*), MF and PF terminal marker VGluT1 (*H*), and serotonergic fiber marker HTT (*I*). *J, K*. Double immunofluorescence for YC (green) and DsRed (red). DsRed was introduced into Golgi cell (*J*) or LC (*K*) by *in utero* electroporation at E14.5. Note dense inputs of DsRed(+) Golgi cell terminals on to YC(+) LC dendrites (enlarged in inset), and of YC(+) LC terminals on to DsRed(+) Golgi cell soma and dendrites (*J*). Also note dense inputs of DsRed(+)/YC(+) LC terminals on to DsRed(-)/YC(+) LC dendrites (inset, *K*). Asterisks indicate the soma of YC(+) LCs. *A-J* are images taken from sagittal cerebellar sections, and *K* from a plane tangential to the PC layer in coronal cerebellar section. *L*. Box plots showing the number of inputs from granule cells (GrC), CFs, MFs, PCs and inhibitory interneurons in the granular layer (GLI) per 1 μm on the dendritic (left) and somatic (right) surface of YC(+) LCs. Box plots display median, 25^{th} and 75^{th} percentiles and whisker boundaries indicate the 10^{th} and 90^{th} percentiles. *M-P*. Scatter plots showing the density (N/μm) of terminals onto individual LC dendrites (> 10 μm in length, circles) and soma (triangles). Each set of plots indicates the relationship between total excitatory (VGluT1(+) or VGluT2(+)) terminals vs. total inhibitory (VIAAT(+)) terminals (*M*), PC (calbindin(+)/VIAAT(+)) terminals vs. GLI (calbindin(-)/VIAAT(+)) terminals (*N*), CF

(small VGluT2(+)) terminals vs. MF (huge VGluT1(+), VGluT2(+), or VGluT1(+)/VGluT2 (+)) terminals (*O*), or CF terminals vs granule cell (small VGluT1(+) terminals) (*P*). Solid and broken lines are fitted lines for plots from dendritic and somatic domains, respectively. *, $p < 0.05$; **, $p < 0.001$, in Pearson's correlation analysis. Detailed values are summarized in Table 2. g, glomerulus; p, pinceau formation. See other abbreviations in Fig. 1. Scale bars, *A, C, D*, *J, K*, 20 μm; *B, E-I*, 10 μm; insets in *F-K*, 2 μm.

Fig 4. Double-labeling preembedding immunoelectron microscopy for morphological characterization of contacts between neurochemically/tracer-defined inputs and YC(+) LCs in the granular layer. Neurochemical markers or anterograde tracer BDA were visualized with diffuse DAB precipitates by immunoperoxidase, while YC was with metal particles by silver-enhanced immunogold. Boxed regions in *A, C, E, G, I, K, M, O* are enlarged in *B, D, F, H, J, L*, *N, P* and contacted sites in *B, D, F, H, J, L, N, P* are further enlarged in insets to show the symmetrical (pairs of white arrowheads) or asymmetrical (black arrowheads) type of contacts. To show synaptic profiles clearly, *D, F, H* are enlarged views taken from adjacent sections of *C, E, G*. *A, B*. Symmetrical synapse between calbindin(+) recurrent PC axon (PCt) and YC(+) LC dendrite (LCD). *C, D*. Asymmetrical synapse between BDA(+) MF terminal (MFt) and YC(+) LC dendrite. BDA was injected into the lateral reticular nucleus, one of the precerebellar nuclei projecting MFs. *E, F*. Asymmetrical synapse between BDA(+) CF terminal (CFt) and YC(+) LC dendrite. BDA was injected into the inferior olive. *G, H*. Asymmetrical synapse between VGluT1(+) glutamatergic terminal and YC(+) LC dendrite. From vertical

trajectory in the granular layer, this VGluT1(+) terminal likely represents the ascending axon of granule cells (GCt). *I, J*. Symmetrical synapse between GlyT2(+) glycinergic terminal (presumably, LC or Golgi cell terminal) and YC(+) LC dendrite. *K-N,* Symmetrical synapse between VIAAT(+)/YC(+) LC terminals and YC(+) LC dendrites (*K, L*) or between GlyT2(+)/YC(+) LC terminals and YC(+) LC dendrites (*M, N*). *O, P*. Lack of typical synaptic specializations between HTT(+) serotonergic fiber and YC(+) LC body (LCB). PCB, Purkinje cell body. Scale bars, *A, C, E, G, I, K*, 5 μm; *B, D, F, H, J, L*, 500 nm; Insets, 100 nm.

Fig 5. A dense lattice of transverse and ascending LC axons innervating molecular layer interneurons and Golgi cells in the molecular layer. *A, B*. Triple fluorescent labeling of a horizontal section for YC (green, A_1), DsRed introduced by *in utero* electroporation (red in A_1, and gray in A_2, *B*), and aldolase C (blue, A_1). A YC(+)/DsRed(+) LC is located just beneath the PC layer (arrow) and extends an ascending axon (Aa) heading for the molecular layer, from which the transverse axon (Ta) emits and traverses medio-laterally across several aldolase C(+)(double-headed arrows) and aldolase C(-) stripes. A boxed region in A_2 is enlarged in *B* to show occasional emission of an ascending axon from the transverse axon (arrow). *C*. Emission of LC axons from LD dendrites (arrowheads). Note that LC axon bifurcates into one ascending toward the molecular layer and the other descending toward deep portions of the granular layer. Dendrodendritic contact between YC(+)/DsRed(+) and YC(+)/DsRed(-) LCs (arrows) is also observed. *D, E*. Double immunofluorescence for YC (green) and VIAAT (red, *D*) or GlyT2 (red, *E*) in the molecular layer. All terminal boutons on YC(+) LC axons express VIAAT. YC(+) LC

axons are either positive (arrows) or negative (arrowheads) to GlyT2. *F-H*. Triple labeling for YC (green or gray), parvalbumin (PA, red), and calbindin (blue) showing LC axons, which innervate PA(+)/calbindin(-) molecular layer interneurons (asterisks), but not PA(+)/calbindin(+) PCs. Note that ascending LC axons (Aa) densely innervate somatodendritic elements of individual molecular layer interneurons, while transverse LC axons (Ta) form one or two synapses on them. When using parasagittal sections (*H*) for better tracing of ascending axon trajectory, this axon well embraces the soma and proximal dendrites of molecular layer interneurons. *I*. Double labeling for YC (green or gray) and Golgi cell marker neurogranin (NG, red) showing LC axon innervation of NG(+) Golgi cells. Note both ascending and transverse axons of YC(+) LCs innervate Golgi cell dendrites in the molecular layer. *J-N*. Preembedding immunogold labeling for YC in horizontal cerebellar sections. YC(+) ascending (*J, K*) and transverse (*L-N*) LC axons (LCt) innervates interneuron dendrites (InD) by forming symmetrical synapses (white arrowheads). *M* is an enlarged view taken from adjacent sections corresponding to the boxed region of *L* to clearly show synaptic profiles. Boxed region in *K* and *M* are enlarged in inset (K) or N, respectively, to show symmetrical synaptic contact (white arrowheads). A-B, apico-basal direction. M-L, medio-lateral direction. *O, P*. Double-labeling preembedding immunoelectron microscopy for YC (silver-enhanced immunogold) and neurogranin (DAB precipitates) showing symmetrical synapse formation between YC(+) LC terminals (LCt) and NG(+) Golgi cell dendrite (GoD). Scale bars, *A*, 100 μm; *B*, 20 μm; *C-I*, 10 μm; *J, L*, 2 μm; *K, M, O*, 500 nm; inset in *K*, *N*, *P*, 200 nm.

Fig 6. Compartmentalized arborization of LC dendrites and exclusive inputs from PCs within a given compartment. *A, B*. Merged images (top) of triple immunofluorescence for YC (green, or gray), calbindin (blue) and aldolase C (red), and separated YC images (bottom). Coronal cerebellar sections cut through the PC layer tangentially were imaged from anterior lobule 4/5 (*A*) and posterior lobule 9 (*B*). *C.* Double immunofluorescence for YC (green) and DsRed introduced by *in utero* electroporation (red). Somatodendritic meshwork of LC dendrites is constructed by intimate dendrodendritic and dendrosomatic contacts. *D*. Preembedding silver-enhanced immunogold for YC showing adherens junction formed between apposing YC(+) LC dendrites (LCD). *E*, Box plots showing the mean gray density of YC(+) elements in at aldolase C(+) (red open column), aldolase C(-) (blue open column), and border regions (pink filled column). **, $p < 0.01$, Kruskal Wallis test. *F*. Merged image (top) of triple fluorescent labeling for YC (green), DsRed introduced into LC by *in utero* electroporation (red or gray), and aldolase C (blue) and separated DsR image (bottom). Dotted lines indicate stripe borders. *G* is a high-power image of *F*. Note that most LC dendrites of a DsRed(+)/YC(+) LC (yellow asterisk) are distributed inside an aldolase C(+) stripe (white arrowheads), with a few short dendrites crossing stripe borders (black arrowheads). *H*. Dot plots showing the length ratio of LC dendrites inside a single aldolase C stripe in which the LC soma is located (open red column) or those crossing the border into a neighboring stripe (filled red column). **, $p < 0.01$, Student's *t*-test. *I, J*. Triple immunofluorescence for YC (green), calbindin (blue) and aldolase C (red). *J* is a high-power image of *I*. Somatodendritic elements of YC(+) LC in aldolase C(-) stripe (asterisk) is mainly innervated by aldolaseC (-)/calbindin(+) PC terminals, i.e., neurochemically matched PC terminals and is additionally innervated

by aldolaseC(+) PC terminals, i.e., neurochemically mismatched PC terminals. *K*. Box plots showing the density of matched and mismatched PC terminals. All box plots display median, 25th and 75th percentiles and whisker boundaries indicate the 10th and 90th percentiles. **, $p < 0.01$, Mann-Whitney *U*-test. Scale bars, *A*, *F*, 50 μm; *C, G, I, J* 10 μm; Inset in *C*, 2 μm; *D*, 200 nm.

Fig 7. Organization of LC circuits in the cerebellar cortex. LCs receive various inputs with their *somatodendritic meshwork*, which is interconnected with each other via adherens junctions and mainly extends within a given aldolase C compartment. LC inputs include excitatory inputs from climbing fibers (CF), mossy fibers (MF), and ascending axon of granule cells (GrC), inhibitory inputs from Purkinje cells (PC), Golgi cells (GoC), and Lugaro cells (LC), and serotonergic fibers. LCs project ascending and transverse axons and construct a dense *axonal lattice* casting the entire molecular layer. Both types of LC axons innervate molecular layer interneurons (MLI, i.e., basket and stellate cells) and Golgi cells, but not PCs. The circuit configuration suggests that LCs integrate various inputs coming to the belonging cerebellar compartment and, as an interneuron-selective interneuron, can effectively disinhibit PCs and granule cells in a compartment-dependent manner through inhibition of molecular layer interneurons and Golgi cells, respectively. Furthermore, anchorage of serotonergic fibers to LCs should increase the target specificity and potency of serotonergic modulation to control cerebellar cortical activities. A-B, apico-basal direction. M-L, medio-lateral direction. PF, parallel fiber; R-C, rostro-caudal direction. *B.* LC as a unique interneuron-selective interneuron regulating PC and granule cell activities. Left. The LC-MLI-PC pathway. Through this pathway, LCs

disinhibit PCs via inhibition of molecular layer interneurons and, in turn, PCs inhibit LCs via recurrent PC axons. Right. The LC-GoC-GrC pathway. Through this pathway, LCs disinhibit granule cells (GrC) via inhibition of Golgi cell (GoC)-mediated feed-forward and feed-back inhibitions. Based on this strategic configuration, LCs can effectively modulate cerebellar cortical activities by integrating compartmentalized inputs, and by disinhibiting PCs and granule cells inside, and also beyond, the compartment.

Table 1. Details of the primary antibodies used.

Molecule	Sequence NCBI	Host	Specificity RRID	Reference or company code #
aldolase C	314-363 aa NM 009657	GP	IB-HEK AB_2571660	Tsutsumi et al., 2015
calbindin	1-261 aa NM009788	Go	IB, IHC AB_2571569	Miura et al., 2006
CR	1-271 aa AB037969	Rb	IB, IHC AB_2571666	this study
DsRed	1-225 aa GU253312	Rb	IHC AB_2571647	this study
$GABA_AR\alpha1$	369-386 aa NM_010250	Rb	IB, IB-HEK AB_2571571	(Ichikawa et al., 2011)
GFP	1-238 aa YP_002302326	Rb, Go	IHC AB_2571573 (Rb) AB_2571574 (Go)	(Takasaki et al., 2010)
GlyRα1	380-403 aa NM_020492	Rb	IHC AB_2571772	Frontier Science GlyRa1-Rb-Af840
GlyT2	1-18 aa AF411042	GP	IB, IB-HEK AB_2571607	(Hondo et al., 2011)

HTT	1-77 aa	Rb	IB	(Somogyi et al., 2004)
	AF013604		AB_2571775	
neurogranin	1-78 aa	Rb	IB	(Miyazaki et al., 2011)
	NM_022029		AB_2571811	
pan-AMPAR	717-754 aa	GP	IB, IB-HEK	(Fukaya et al., 2006)
	X57497		AB_2571610	
parvalbumin	1-110 aa	GP	IB	(Nakamura et al., 2004)
	NM_013645		AB_2571615	
3PGDH	1-533 aa	Rb	IB	(Furuya et al., 2000)
	NM031620		AB_2571653	
VGluT1	531–560 aa	Rb	IB	Frontier Science
	BC054462		AB_2571616	VGluT1-Rb-Af500
VGluT2	559 –582 aa	Rb, GP	IB	Frontier Science
	BC038375		AB_2619683 (Rb)	VGluT2-Rb-860
			AB_2571621 (GP)	VGluT2-GP-Af810
VIAAT	31-112 aa	Rb, GP	IB	(Fukudome et al., 2004)
	BC052020		AB_571622 (Rb)	
			AB_2571624 (GP)	

---

aa, amino acid residues; GFP, green fluorescent protein; GFP/UV, green fluorescent protein irradiated by ultraviolet light; GlyRα1, glycine receptor α1 subunit; GlyT2, glycine transporter-2; Go, goat polyclonal antibody; GP, guinea pig polyclonal antibody; HTT, 5-hydroxytryptamine (or serotonin) transporter; IB, immunoblot with brain

homogenates; IB-HEK, immunoblot with HEK293T cell lysates; IHC, cell type-specific immunohistochemical labeling; NCBI, National Center for Biotechnology Information; pan-AMPAR, pan-α amino-3-hydroxy-5-methyl-4-isoxazolepropionic acid receptor; 3-PGDH, 3-phosphoglycerate dehydrogenase; Rb, rabbit polyclonal antibody; RRID, Research Resource Identifier; VGluT1, vesicular glutamate transporter-1; VGluT2, vesicular glutamate transporter-2; VIAAT, vesicular inhibitory amino acid transporter.

Table 2. Details of quantitative analysis for LC inputs

Series (combination of antibodies)	LC dendrite	LC soma
Terminal	density (N/μm)	density (N/μm)
	n	n
	measured length	measured length
Series 1 (VIAAT/VGluT1+2/YC)		
Inhibitory	0.32 ± 0.02	0.13 ± 0.01
Excitatory	0.29 ± 0.01	0.14 ± 0.01
	87 dendrites	89 somata
	5332.4 μm	3762.4 μm
Series 2 (Calbindin/VIAAT/YC)		
PC axon	0.13 ± 0.01	0.07 ± 0.01
GLI	0.13 ± 0.01	0.06 ± 0.01
	76 dendrites	89 somata
	3645.7 μm	3026.2 μm
Series 3 (VGluT1/VGluT2/YC)		
Granule cell axon	0.13 ± 0.02	0.05 ± 0.01
CF	0.12 ± 0.01	0.05 ± 0.01
MF	0.13 ± 0.01	0.05 ± 0.01

	45 dendrites	46 somata
	2029.7 μm	1660.3 μm

Pearson's correlation analysis

Set of plots	r value	p value	number of plots
Excitatory vs Inhibitory @dendrite	0.49	1.6×10^{-6}	87
Excitatory vs Inhibitory @soma	0.37	4.0×10^{-4}	89
PC vs GLI @dendrite	-0.45	5.2×10^{-5}	76
PC vs GLI @soma	-0.48	2.1×10^{-6}	89
CF vs MF @dendrite	-0.34	0.024	45
CF vs MF @soma	-0.17	0.26	46
CF vs Granule cell axon @dendrite	0.40	7.2×10^{-3}	45
CF vs Granule cell axon @soma	-0.14	0.37	46

CF, climbing fiber; GLI, inhibitory interneurons in the granular layer; MF, mossy fiber; PC, Purkinje cell;

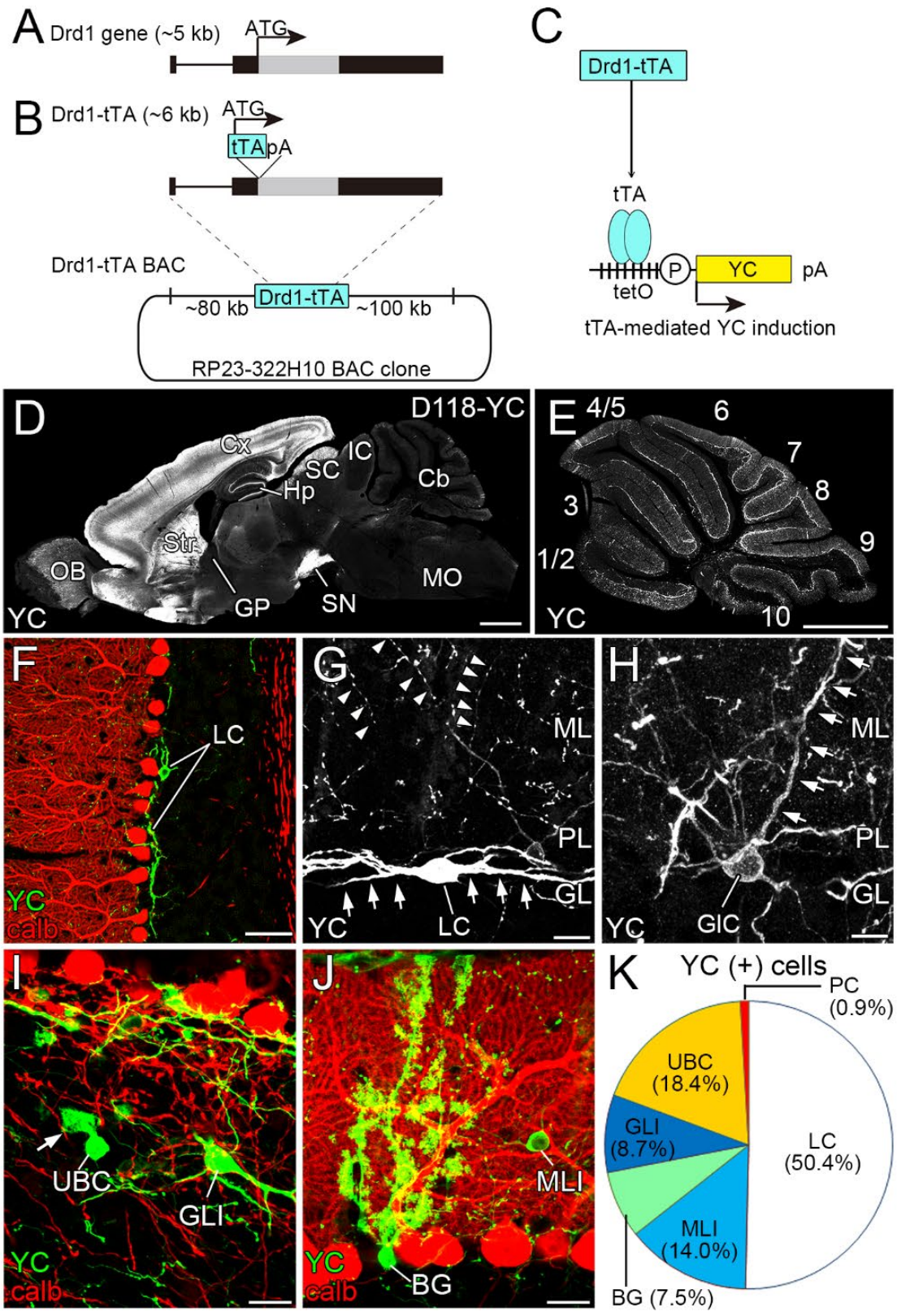

Miyazaki et al Fig. 1

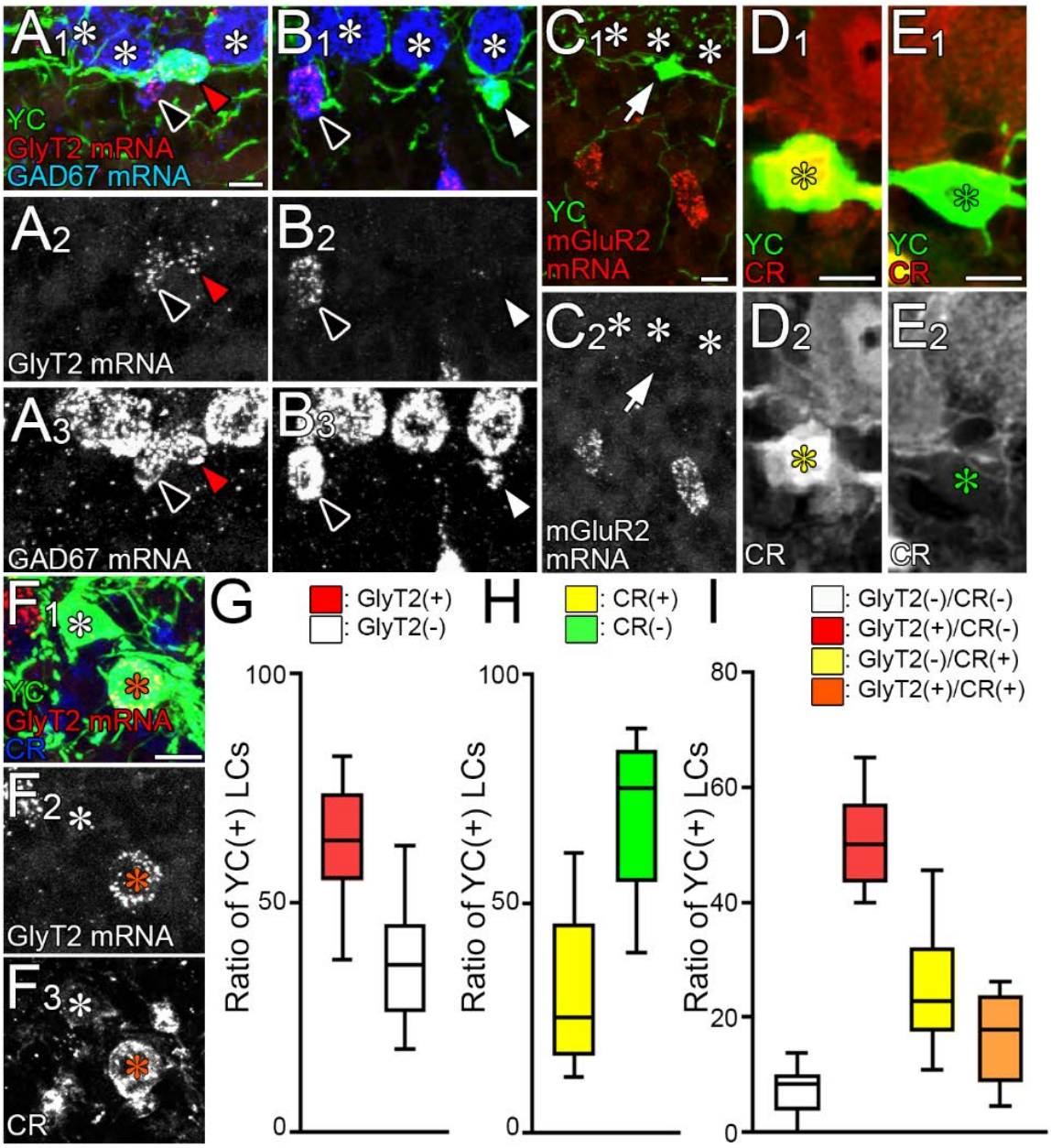

Miyazaki et al Fig. 2

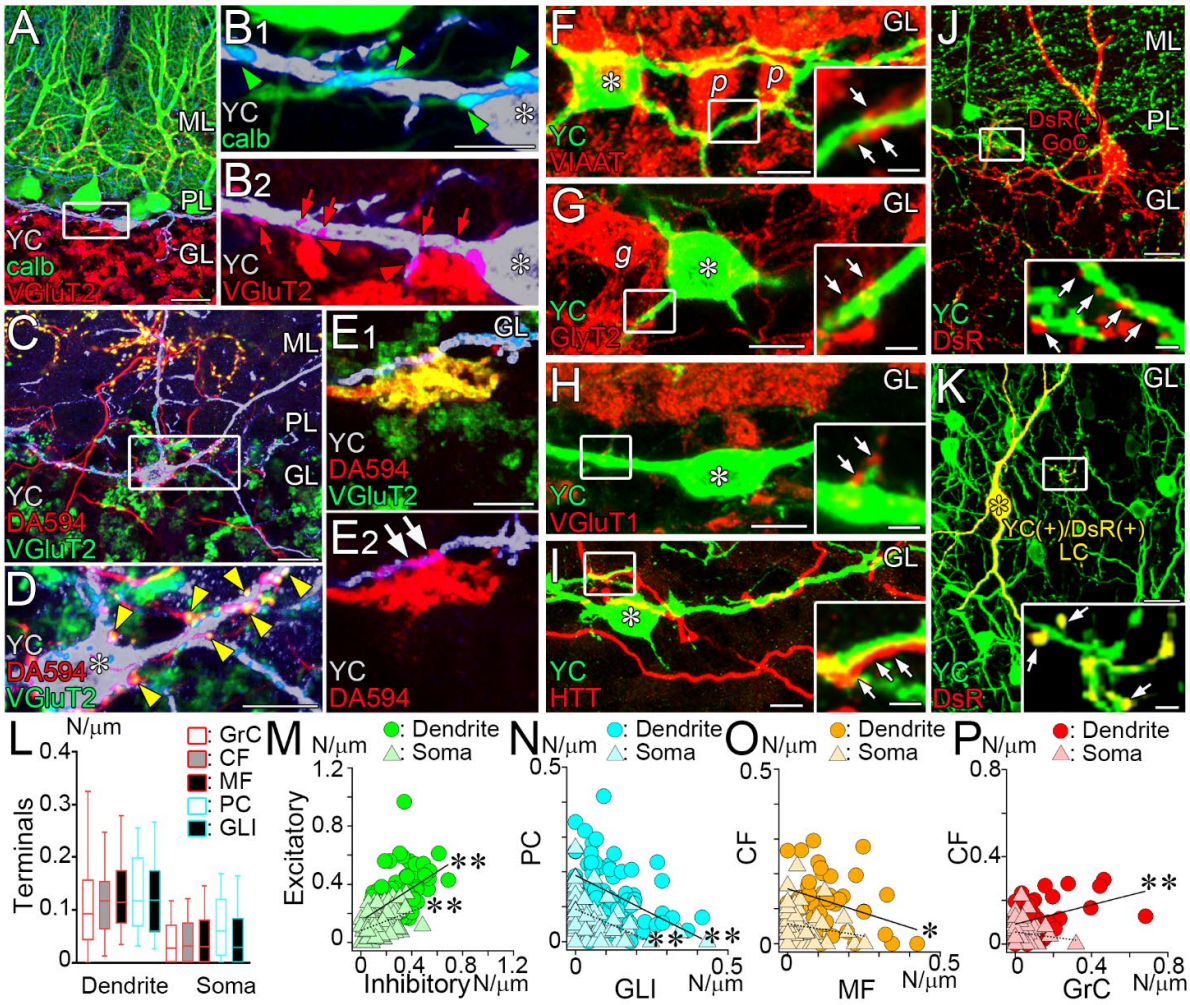

Miyazaki et al Fig. 3

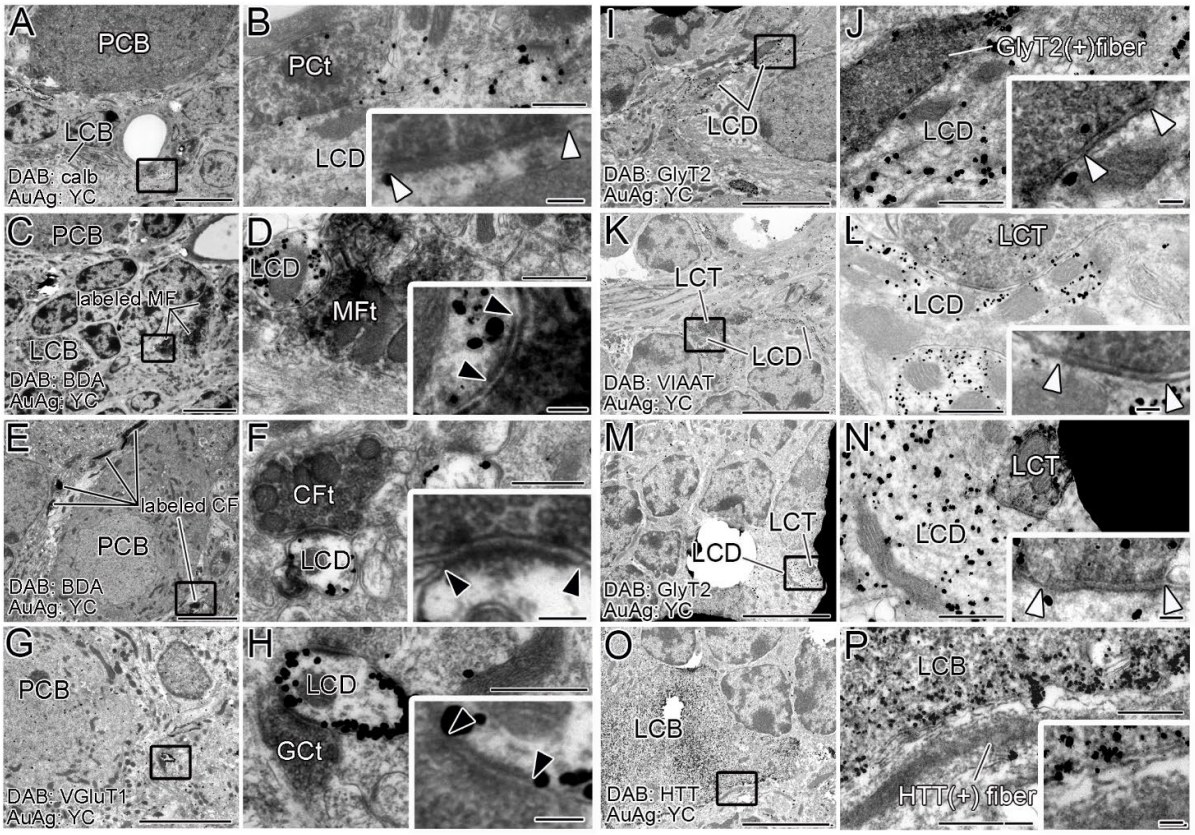

Miyazaki et al Fig. 4

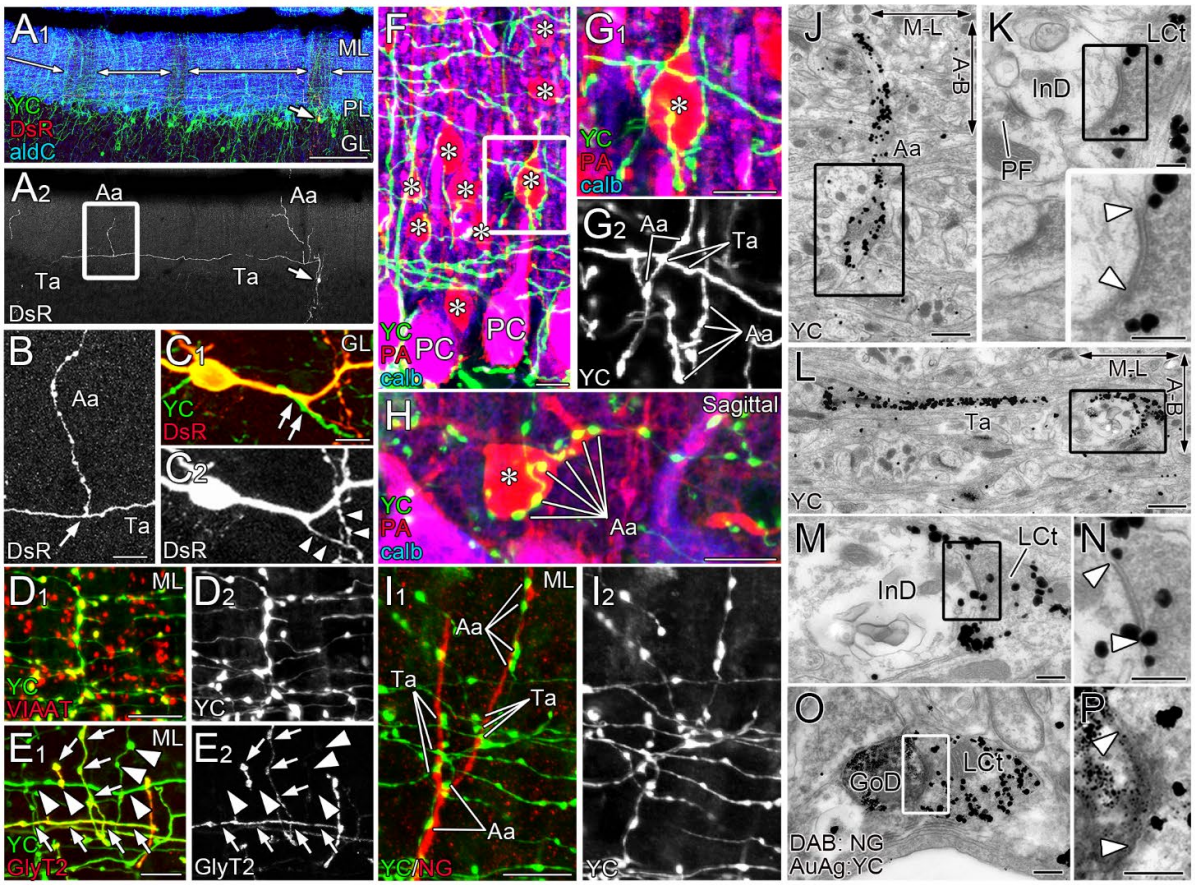

Miyazaki et al Fig. 5

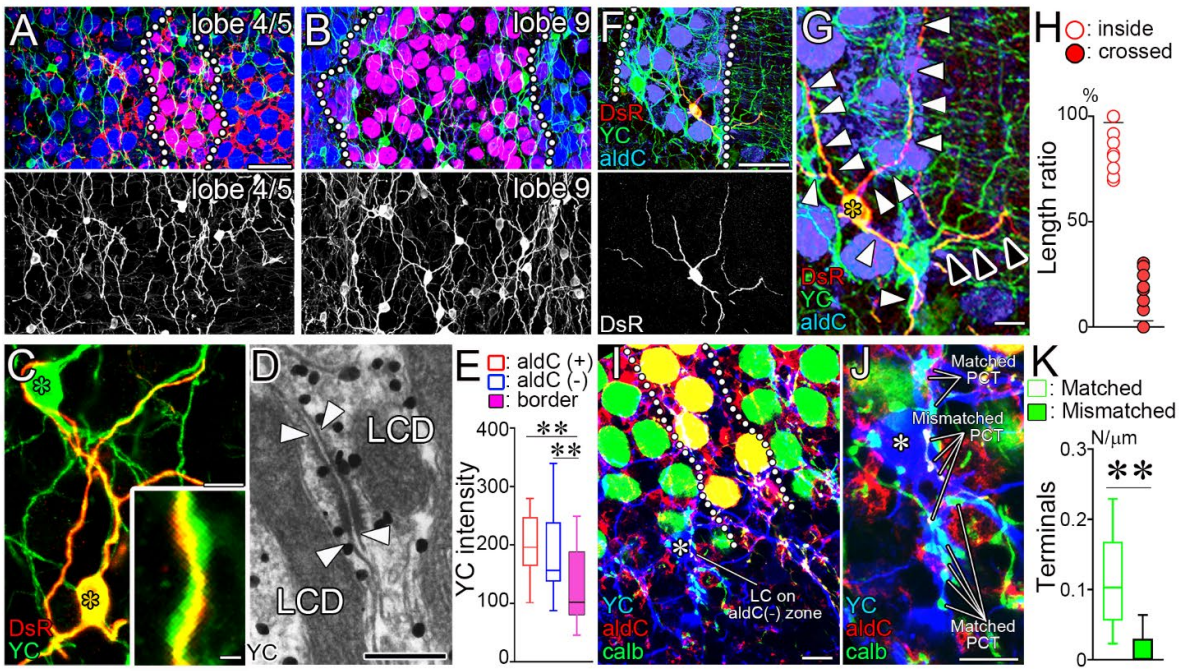

Miyazaki et al Fig. 6

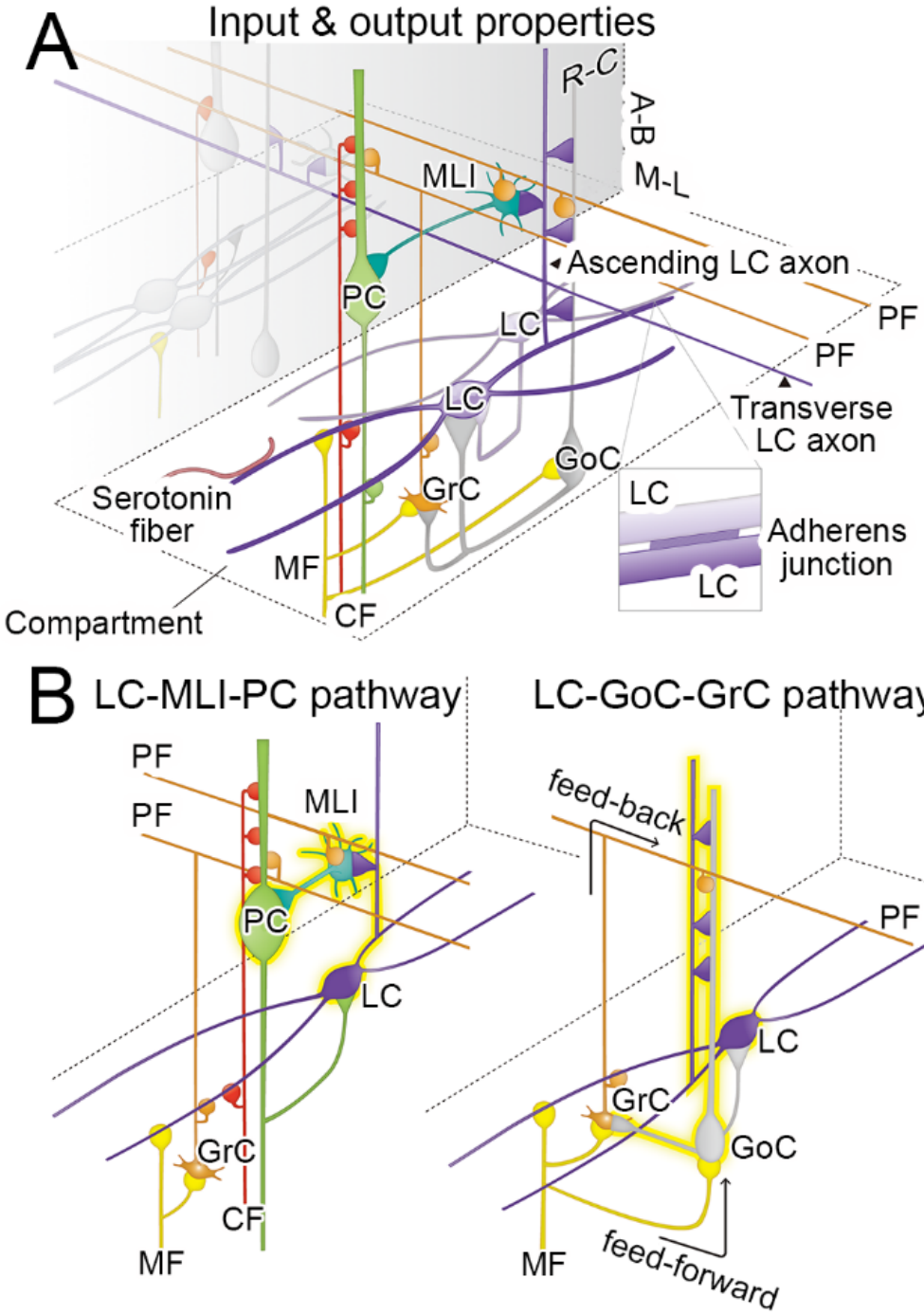

Miyazaki et al Fig. 7